Smart Materials and Structures

PAPER

A hyperelastic porous media framework for ionic polymer-metal composite actuators and sensors: thermodynamically consistent formulation and nondimensionalization of the field equations

To cite this article: Zakai J Olsen and Kwang J Kim 2021 *Smart Mater. Struct.* **30** 095024

IOP Publishing Smart Materials and Structures
Smart Mater. Struct. **30** (2021) 095024 (26pp) https://doi.org/10.1088/1361-665X/ac17a1

A hyperelastic porous media framework for ionic polymer-metal composite actuators and sensors: thermodynamically consistent formulation and nondimensionalization of the field equations

Zakai J Olsen and Kwang J Kim*

Active Materials and Smart Living (AMSL) Lab, Department of Mechanical Engineering, University of Nevada Las Vegas, Las Vegas, NV, United States of America

E-mail: kwang.kim@unlv.edu

Received 28 May 2021, revised 20 July 2021
Accepted for publication 26 July 2021
Published 18 August 2021

Abstract

Ionic polymer-metal composites (IPMCs) are smart materials that exhibit large deformation in response to small applied voltages, and conversely generate detectable electrical signals in response to mechanical deformations. The study of IPMC materials is a rich field of research, and an interesting intersection of material science, electrochemistry, continuum mechanics, and thermodynamics. Due to their electromechanical and mechanoelectrical transduction capabilities, IPMCs find many applications in robotics, soft robotics, artificial muscles, and biomimetics. The current literature is sparce in multiphysics models that account for large deformations, coupled ion-solvent transport, the porous structure of the membrane, and lossy electrodes under finite-strains. This study addresses this by developing a new, hyperelastic porous media modeling framework for IPMCs using the principles of continuum thermodynamics and multiphasic materials. This framework compactly captures the broadest strokes of IPMC modeling methodologies, summarizing them in the form of general constitutive requirements placed on thermodynamic potential describing the polymer skeleton. A simple IPMC model is derived under this framework which captures the finite-strain deformation of a hyperelastic material, accounting for the coupled ion-solvent transport through the porous polymer, and resistive electrodes deforming with the skeleton. The resulting governing equations are further cast into a generalized nondimensional formulation, and an expansive set of unique dimensionless Π-groups are derived for IPMC actuator and sensor devices. This new framework and the nondimensional formulation lay the groundwork for future research and an expansive characterization of IPMC transduction phenomena via dimensional analysis.

* Author to whom any correspondence should be addressed.

Keywords: soft-robotics, ionic polymer-metal composites, electroactive polymers, dimensional analysis, continuum mechanics

(Some figures may appear in colour only in the online journal)

Nomenclature

Fields, parameters, and operators

Quantity	*SI Units*	*Description*
$\underline{a}$	$[\mathrm{m\,s^{-2}}]$	Acceleration/mass weighted acceleration (no subscript)
$\underline{b}$	[N]	Body force
c, C	$[\mathrm{mol\,m^{-3}}]$	Spatial/Material molar concentration
$\mathcal{C}_i$	[□]	Material modulus (denoted by index setin subscripts)
curl, Curl, $\nabla\times$	$[\mathrm{1\,m^{-1}}]$	Spatial/Material/Infinitesimal curl operator
div, Div, $\nabla\cdot$	$[\mathrm{1\,m^{-1}}]$	Spatial/Material/Infinitesimal divergence operator
div_S, Div_S, $\nabla_S\cdot$	$[\mathrm{1\,m^{-1}}]$	Spatial/Material/Infinitesimal surface divergence operator
$\mathcal{D}_{ij}$	$[\mathrm{m^2\,s^{-1}}]$	Diffusivity of i w.r.t. j
$\mathrm{d}\Omega$	$[\mathrm{m^3}]$	Differential element of domain
$\mathrm{d}S$	$[\mathrm{m^2}]$	Differential element of boundary
$\mathrm{d}\ell$	[m]	Differential element of curve/path
Δ	[−]	Dimensionless actuation displacement
$\underline{d}, \underline{D}$	$[\mathrm{C\,m^{-2}}]$	Spatial/Material electric displacement
$\underline{\underline{D}}$	$[\mathrm{1\,s^{-1}}]$	Symmetric spatial velocity gradient
ϵ	$[\mathrm{F\,m^{-1}}]$	Dielectric constant
ε_V	[−]	Volumetric strain
$\underline{e}, \underline{E}$	$[\mathrm{V\,m^{-1}}]$	Spatial/Material electric field
$\underline{\underline{E}}$	[−]	Green-Lagrange strain tensor
$\underline{\underline{\varepsilon}}$	[−]	Infinitesimal strain tensor
$\mathcal{F}$	$[\mathrm{C\,mol^{-1}}]$	Faraday's constant
$\underline{\underline{F}}$	[−]	Deformation gradient
grad, Grad, ∇	$[\mathrm{1\,m^{-1}}]$	Spatial/Material/Infinitesimal gradient operator
grad_S, Grad_S, ∇_S	$[\mathrm{1\,m^{-1}}]$	Spatial/Material/Infinitesimal surface gradient operator
$\tilde{\mathscr{G}}_f$	$[\mathrm{J\,kg^{-1}}]$	Fluid Gibbs free energy per fluid mass
H	$[\mathrm{1\,m^{-1}}]$	Mean surface curvature
$\underline{h}, \underline{H}$	$[\square\cdot\mathrm{m\,s^{-1}}]$	Spatial/Material flux
$\mathscr{h}$	$[\mathrm{J\,m^{-3}}]$	Enthalpy
I_{sc}, $I_\pm$	[A]	Short-circuit current, Upper (+)/ lower(−) clamp current
$\underline{i}, \underline{I}$	$[\mathrm{A\,m^{-2}}]$	Spatial/Material ionomer current density
$\underline{i}^S, \underline{I}^S$	$[\mathrm{A\,m^{-1}}]$	Spatial/Material surface electrode current density
$\underline{\underline{I}}$	[−]	Identity tensor
J, J_s	[−]	Deformation gradient Jacobian/ Skeletal volume weighted
$\underline{j}, \underline{J}$	$[\mathrm{A\,m^{-2}}]$	Spatial/Material current density
k_f	$[\mathrm{m^2\,s^{-1}\,Pa}]$	Hydraulic permeability
$\mathcal{K}$	[J]	Total kinetic energy
λ, Λ	[−]	Spatial/Material volume fraction
λ_d	[m]	Debye screening length
$\underline{\underline{m}}_{mn}, \underline{\underline{M}}_{mn}$	[−]	Spatial/Material Onsager tensor coefficients
μ	$[\mathrm{J\,mol^{-1}}]$	Chemical potential
n_{dw}, n_{d+}	[−]	Water/Ion transference coefficient
ν	$[\mathrm{m^3\,mol^{-1}}]$	Molar volume of fluid constituent
$\underline{n}, \underline{N}$	[−]	Spatial/Material surface normal vector
$\Omega_{0,t}, \partial\Omega_{0,t}$	[−]	Domain/Domain boundary (Material, Spatial)
p	[Pa]	Hydrostatic pore pressure
p	[Pa]	Conjugate pressure
$\mathscr{p}$	[Pa]	Lagrange multiplier (Lagrange pressure)
Π	[−]	Dimensionless group
$\underline{\underline{\mathbb{P}}}, \underline{\underline{\overline{\mathbb{P}}}}$	[−]	Spatial/Material surface projection tensor
ψ, Ψ	$[\mathrm{J\,m^{-3}}]$	Spatial/Material Helmholtz free energy
ϕ	[V]	Electric potential
$\phi_{\mathrm{oc}}, \phi_\pm$	[V]	Open-circuit voltage, Upper (+)/lower (−) clamp potential
Q	$[\mathrm{J\,s^{-1}}]$	Total heat supply
q	$[\mathrm{J\,m^{-3}\,s}]$	Volumetric heat source
$\mathscr{q}$,$\mathscr{q}_0$	[C]	Total electrical charge/electron charge
R	[J mol K]	Universal gas constant
ρ^*	$[\mathrm{kg\,m^{-3}}]$	Intrinsic mass density
ρ	$[\mathrm{kg\,m^{-3}}]$	Apparent (w/subscript)/(w/o subscript) total mass density
r	$[\square\,\mathrm{m^{-3}}]$	Volume supply heat/entropy
$\underline{r}$	[m]	Spatial position vector
$\underline{\underline{r}}_e, \underline{\underline{R}}_e$	[Ω m]	Spatial/Material electrode resistivity
$\mathscr{s}, \mathcal{S}$	$[\mathrm{J\,m^{-3}\,K}]$	Spatial/Material entropy density
$\mathscr{z}$	$[\mathrm{J\,K^{-1}}]$	Total entropy
$\underline{\underline{S}}$	[Pa]	Second Piola–Kirchhoff stress tensor
$\underline{\underline{\sigma}}_e, \underline{\underline{\Sigma}}_e$	$[\mathrm{S\,m^{-1}}]$	Spatial/Material electrode conductivity
$\underline{\underline{\sigma}}, \underline{\underline{\sigma}}_f$	[Pa]	Cauchy stress tensor/Fluid stress tensor(spatial)
t	[s]	Time
τ	[s]	Timescale (in dimensional analysis)
T	[Θ]	Thermodynamic temperature
$\underline{t}$	[Pa]	Spatial surface traction vector
$\underline{u}$	[m]	Displacement field
$\mathscr{u}, \overline{\mathscr{u}}$	$[\mathrm{J\,m^{-3}}]$	Spatial internal energy density/total internal energy
$\underline{v}$	$[\mathrm{m\,s^{-1}}]$	Velocity field
$\mathscr{w}, \mathscr{w}$	$[\mathrm{C\,m^{-2}}]$	Spatial/Material surface charge
W	[J]	Work
$\underline{w}$	$[\mathrm{m\,s^{-1}}]$	Filtration velocity
$\underline{x}, \underline{X}$	[m]	Spatial/Material coordinate
z	[−]	Charge number

*the notation '[□]' indicates units depend on particular quantity in question

Subscripts

a	Applied value (boundary conditions)
α	Constituent phase of combined medium
β	Constituent phase of bulk fluid
c	Characteristic field value (in dimensional analysis)
ext	External (work/work rates)
elec	Electrical (work/work rate)
f	Bulk fluid phase
s	Solid phase
$\dot{s}$	Entropy (source, flux)
w	Solvent water species
q	Heat (source, flux)
$+$	Cation species/Upper electrode interface
$-$	Anion species/Lower electrode interface
0	Initial/reference quantity
$\alpha*$	Per mass of phase α
$\{E, \nu, \lambda, \mu, K, M, \mathcal{B}\}$	Material moduli (Young, Poisson, Lamé 1, Lamé 2, Bulk, P-wave, Beam)

Superscripts

f	Fluid based/referenced quantity
S	Superficial quantity
T	Transpose (of a tensor/vector quantity)
$*$	Intrinsic property

Accents/bracket operators

$\bar{\square}$	Volume integrated quantity
$\widehat{\square}$	Dimensionless field variable
$[\square]$	Matrix quantity
$\{\square\}$	Set of quantities
$\|\square\|$	Surface jump in argument

1. Introduction

1.1. Ionic polymer-metal composite materials

Ionic polymer-metal composites (IPMCs) are a class of highly functional smart materials called electroactive polymers (EAPs). These materials exhibit a mechanical response to electrical inputs, (electromechanical transduction) and conversely an electrical response to mechanical input, (mechanoelectrical transduction) [1–3]. These energy transduction capabilities allow EAP materials to be used as both actuators (electromechanical), and sensors (mechanoelectrical), and hence find many applications in robotics, soft robotics, wearable technology, and biomimetics.

The IPMC in particular shows great promise for the future of robotic engineering and design. These materials demonstrate large deformations in response to low voltage electrical inputs (0.5–2 V), relatively fast response speed (0.1–5 Hz), and operate in underwater environments [4–6]. The history of IPMC literature is rich in survey and review material which capture the evolution of IPMC modeling and applications over time [7–12].

The typical structure of an IPMC consists of a polymeric membrane with selective ion transport capabilities (i.e. an ionic exchange membrane) composited between layers of conducting electrode material [7, 13–18]. Two common ionic polymers (ionomers) used in the fabrication of IPMCs are Nafion and Aquivion [19, 20], while the electrodes are commonly made from chemically plated noble metals such as gold and platinum [7, 8, 13]. The ionomeric polymers used in IPMCs exhibit an ionic clustering morphology, wherein anions fixed to the polymer backbone arrange themselves into ionic clusters, forming a porous network containing solvent and neutralizing cations.

1.2. Transduction phenomena and multiphysics modeling of IPMCs

The fundamental principal underpinning IPMC transduction is the existence of fixed charges attached to the ionomer backbone and mobile charges within the interstitial porous structure of the membrane. Under an applied electric field, the mobile cation species migrate to the cathode due to electromigration, and with them some solvent water molecules are dragged due to ionic hydration [21–28]. This concentration imbalance in the cation species generates an osmotic pressure that works in conjunction with electrostatic effects due to charge redistribution to deform the IPMC [29–34]. Conversely, mechanically deforming the material generates a volumetric strain and convective-diffusive migration effects for the bulk solvent and ionic solute species, inducing a net charge imbalance and detectable electrical signals in the electrodes [3, 30, 35–40].

An illustration of these two distinct modes of transduction is presented in figure 1. One important note is the mechano-electrical transduction behavior of an IPMC is dependent on the circuit conditions of the electrodes. In an open-circuit configuration, the IPMC produces a detectable electric potential but no current flow through the IPMC at the electrodes. Conversely, in a short-circuit configuration the electrodes maintain the same floating potential and the IPMC produces a sensing current through the electrodes.

There exist many modeling frameworks for IPMC transduction in the literature. Some approaches are based on an analysis of the microstructure of the polymer [32, 41], while others utilize classical transport equations, such as the Poisson–Nernst–Planck equations, and the principles of structural mechanics to create a multiphysics model of IPMC transduction [21, 42–48]. More recent works leverage continuum thermodynamics to construct models that are derivable from potential functions [33, 49–53]. What all of these have in common is their goal of coupling the electrochemistry of migrating ionic species to the mechanical deformation of a solid structure.

The field of soft robotics and biomimetics relies heavily on EAP actuators and sensors, and IPMCs are a strong candidate for many applications currently being developed. As

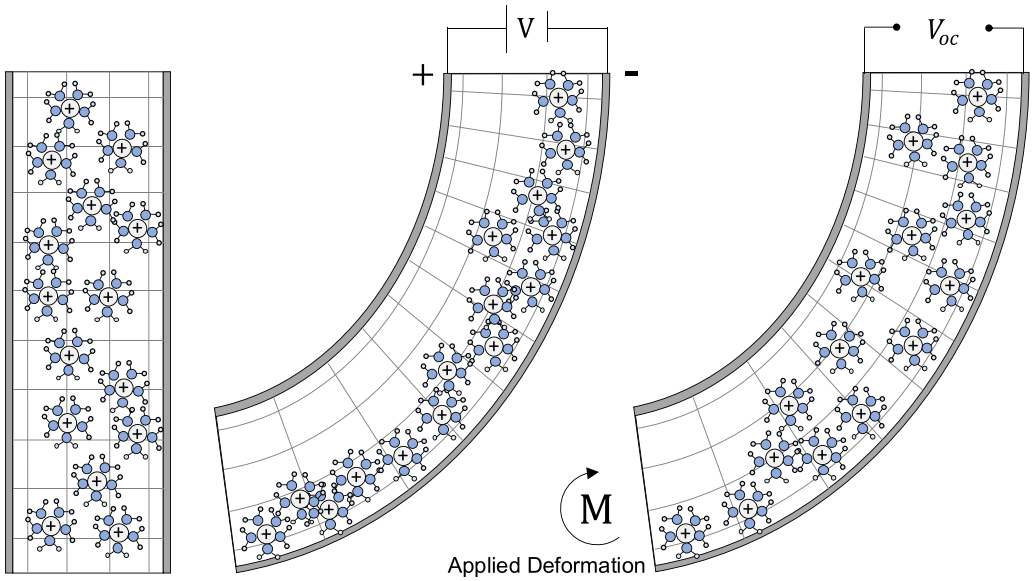

Figure 1. Illustration of IPMC transduction modes. (Left) A static IPMC with no applied voltage or deformation; the entire polymer domain remains electroneutral. (Center) Electromechanical transduction of an IPMC, wherein an applied voltage induces hydrated cation redistribution to the cathode, resulting in deformation of the composite material. (Right) Mechanoelectrical transduction of the IPMC, wherein the applied deformation, illustrated as a bending moment, creates ionic redistribution, and induces an open-circuit potential.

both actuators and sensors, IPMCs provide interesting benefits for robotic and soft robotic systems due to their flexibility, large deformations, small actuating voltages, and ability to operate underwater. With their many potential applications, it is crucial to have accurate models for IPMCs in both actuation and sensing so that their behavior may be understood and predicted. This is critical for designing applications of IPMCs as well as constructing controllers and control schemes that are suitable for the complex transduction behavior of these materials.

While some works explicitly examine a porous media perspective of IPMCs [39, 54–56], they have not been utilized to conduct an in-depth analysis of the dominant behaviors under both electromechanical and mechanoelectrical transduction. Furthermore, models that account for non-ideal (lossy) electrode have been resigned to infinitesimal strain formulations and there is currently no unifying model of non-ideal electrodes in a finite-strain framework. The porous nature of the ionomeric membranes necessitates models that can account for this structure while also providing the ability to incorporate other complex attributes such as hyperelastic material models, kinematic nonlinearity, and electrostatic interactions or steric effects of ionic solutions.

This work develops such a model, aimed at providing a comprehensive framework for deriving governing partial differential equations (PDEs) that account for the porous ionomer, coupled ion/solvent transport, hyperelastic material models, and interfacial charge transport under large deformations. In this paper, we present a thermodynamically consistent model formulation under finite-strain deformations and provide a comprehensive set of dimensionless Π-groups and complete nondimensionalization of the field equation in the kinematically linearized model.

2. A finite-strain, multiphasic porous media model for IPMC materials

The derivation methodology of our model follows closely with classical continuum mechanics under finite deformation. As such, we have a distinction between material (Lagrangian) and spatial (Eulerian) frames, denoted here by using upper- and lower-case field variables, respectively, when possible. Some fields have unique representations in the material and spatial description and those will be made clear in the text on a case-by-case basis. The tensor rank (scalar/rank-0, vector/rank-1, tensor/rank-2) of a field will be distinguished by use of under bars numbering the rank. The differential operators in the material and spatial frames will also be distinguished via the letter case of the operator; unless the two frames coincide (i.e. under the assumption of small displacements and rotations), in which case the nabla operator will be used. The under bar is not explicitly written for the whole expression for differential operators and the tensor order is inferred by the argument of the operator.

The foundation of the model derivation lies in constructing the balance laws in continuum mechanics and leveraging the first and second laws of thermodynamics to determine the constitutive requirements of the material. This approach is augmented by accounting for the multiphasic nature of the material, the electrochemical aspects of the IPMC, and relates the evolution of the system in space to the deformation of the solid polymer skeleton akin to what is found in literature [57–59], and formalized here for IPMC materials.

2.1. Multiphasic continua

In the description of our multiphasic model, the phase relationship of a field variable is denoted by a corresponding subscript.

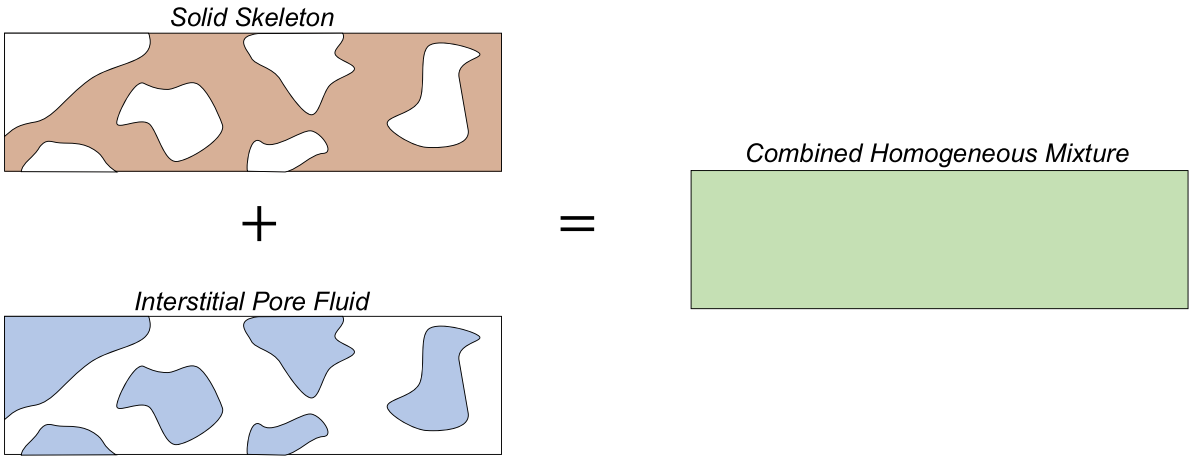

Figure 2. Illustration of multiphasic homogeneous mixture. The solid skeleton (red) and interstitial pore (blue) fluid exist as their own phases within the porous medium. The continuum multiphasic modeling approach tracks these phases using their volume fraction within a combined homogenous mixture (green).

The phases are superimposed upon one another, illustrated in figure 2, each following their own trajectory according to their given displacement field. The combine porous medium is made up of a solid skeleton and a pore fluid. The skeleton consists of the polymer backbone as well as volume-free fixed charges whereas the pore fluid is made up of a miscible mixture of charged and uncharged species [57]. The solid skeleton and pore fluid are treated as a homogenous mixture and are tracked via their volume fractions. By treating the combined medium as a homogenous mixture and following the phases via their volume fractions, we can effectively capture the macroscopic behavior of the IPMC without the need for a detailed model of the microstructure and interfacial phenomena between the polymer and pore fluid.

The intrinsic density of a constituent is denoted as ρ_α^* and is a measure of the mass of the constituent per volume of constituent. A constituent's intrinsic density is related to its apparent density, ρ_α, which measures the mass of constituent per total volume of the porous medium. This relationship is achieved through the volume fraction λ_α.

$$\lambda_\alpha = \frac{\mathrm{d}\omega_\alpha}{\mathrm{d}\omega} \tag{2.1a}$$

$$\rho_\alpha = \lambda_\alpha \rho_\alpha^*. \tag{2.1b}$$

The total mass density of the combined medium is then defined as

$$\rho = \sum_\alpha \rho_\alpha = \sum_\alpha \lambda_\alpha \rho_\alpha^*. \tag{2.2}$$

whereas the overall fluid density takes a summation over all constituent fluid species β.

$$\rho_f = \sum_\beta \rho_\beta = \sum_\beta \lambda_\beta \rho_\beta^*. \tag{2.3}$$

For the constituent fluid species, it will be convenient to work in terms of the molar concentration with respect to either the fluid volume, c_β^f, or volume of the combined homogenous medium, c_β. These are related by the fluid phase volume fraction.

$$c_\beta = \lambda_f c_\beta^f. \tag{2.4}$$

We will be relating the transport of each constituent species with respect to the deforming solid polymer. Thus, we now introduce the filtration velocities of the fluid phase and of the fluid constituent species:

$$\underline{w}_f = \underline{v}_f - \underline{v}_s \tag{2.5a}$$

$$\underline{w}_\beta = \underline{v}_\beta - \underline{v}_s. \tag{2.5b}$$

These velocity definitions are useful when writing the evolution of a field relative to the evolution of the solid phase. For example, the material derivative following a constituent species may be written in relation to the material derivative following the solid phase and the species' filtration velocity.

$$\frac{\mathrm{d}_\alpha(\square)}{\mathrm{d}t} = \frac{\mathrm{d}_s(\square)}{\mathrm{d}t} + \mathrm{grad}(\square)\cdot\underline{w}_\alpha. \tag{2.6}$$

This is effectively an arbitrary Lagrangian–Eulerian formulation which uses the moving skeletal frame as a reference configuration for the mesh. From here on, the material derivative written without any subscript is assumed to follow the skeletal phase.

$$\frac{\mathrm{d}}{\mathrm{d}t}(\square) := \frac{\mathrm{d}_s}{\mathrm{d}t}(\square). \tag{2.7}$$

2.2. The conservation laws of mechanics

2.2.1. Conservation of mass. We consider the conservation of mass for two phases in the porous medium; The skeletal phase, denoted with a subscript s, and the fluid phase, denoted with a subscript f, each with their own apparent densities,

ρ_s and ρ_f, respectively. The fluid phase occupies a volume fraction, $\lambda_f = \lambda$, in the spatial description which denotes the current porosity of the medium. Conservation of mass for the skeletal phase is expressed as the material derivative of skeletal mass density integrated over the spatial volume moving with the solid phase.

$$\frac{\mathrm{d}}{\mathrm{d}t}\int_{\Omega_t} \rho_s \mathrm{d}\Omega = 0 \tag{2.8a}$$

$$\frac{\partial \rho_s}{\partial t} + \mathrm{div}\left(\rho_s \underline{v}_s\right) = 0. \tag{2.8b}$$

The result is a global (integral—(equation 2.8*a*)) and local (differential—(equation 2.8*b*)) statement of the conservation of mass for the solid skeleton. For the fluid mass we formulate the global conservation of mass equation following the deformation of the skeletal phase, and hence we account for mass flux across the boundary of the spatial volume due to fluid flow relative to the skeletal frame.

$$\frac{\mathrm{d}}{\mathrm{d}t}\int_{\Omega_t} \rho_f \mathrm{d}\Omega = -\int_{\partial\Omega_t} \underline{h}_f \cdot \underline{n} \mathrm{d}S. \tag{2.9}$$

The relative mass flux is calculated from the filtration velocity as $\underline{h}_f = \rho_f \underline{w}_f$ [58]. The local mass balance of the fluid can then be written in the spatial frame using the filtration velocity or the relative mass flux.

$$\frac{\partial \rho_f}{\partial t} + \mathrm{div}\left(\rho_f \underline{v}_s\right) = -\mathrm{div}\left(\underline{h}_f\right). \tag{2.10}$$

The saturation condition of the combined medium places a restriction on the volume fractions of the two phases, requiring they add to unity. Thus, the solid and fluid volume fractions are related to the porosity of the combined medium and we only need to track the one field variable, namely porosity.

$$\sum_\alpha \lambda_\alpha = \lambda_s + \lambda_f = 1 \tag{2.11a}$$

$$\lambda_f = \lambda, \quad \lambda_s = 1 - \lambda. \tag{2.11b}$$

The acceleration of each phase is obtained by taking the phase specific material derivative of the velocity.

$$\underline{a}_s = \frac{\mathrm{d}\underline{v}_s}{\mathrm{d}t} = \frac{\partial \underline{v}_s}{\partial t} + \mathrm{grad}\left(\underline{v}_s\right) \cdot \underline{v}_s \tag{2.12a}$$

$$\underline{a}_f = \frac{\mathrm{d}_f \underline{v}_f}{\mathrm{d}t} = \frac{\partial \underline{v}_f}{\partial t} + \mathrm{grad}\left(\underline{v}_f\right) \cdot \underline{v}_f. \tag{2.12b}$$

2.2.2. Conservation of linear momentum. We next apply the principle of balance of linear momentum, wherein we have the body load $\bar{b}$, in units of force per unit mass, and surface traction $\bar{t}$ that are experienced across both phases.

$$\begin{aligned}&\frac{\mathrm{d}}{\mathrm{d}t}\int_{\Omega_t} \rho_s^*\left(1-\lambda\right)\underline{v}_s + \rho_f^*\lambda\underline{v}_f \mathrm{d}\Omega \\ &= -\int_{\partial\Omega_t}\left(\rho_f^*\lambda\underline{v}_f \otimes \underline{w}_f\right)\underline{n}\mathrm{d}S + \int_{\Omega_t}\rho\underline{b}\mathrm{d}\Omega + \int_{\partial\Omega_t}\underline{t}\mathrm{d}S.\end{aligned} \tag{2.13}$$

We follow the deformation of the skeletal phase and account for the additional momentum flux due to relative fluid motion as a separate contribution, seen in the first term on the right-hand-side (RHS), wherein $\otimes$ denotes the tensor product. We introduce the Cauchy stress tensor, $\underline{\underline{\sigma}}$, which maps a surface normal, $\underline{n}$, to the traction vector acting on that surface via $\underline{t} = \underline{\underline{\sigma}}\underline{n}$. The stress tensor, combined with mass conservation, allow us to form the local balance of linear momentum.

$$\rho_s^*\left(1-\lambda\right)\underline{a}_s + \rho_f^*\lambda\underline{a}_f - \mathrm{div}\left(\underline{\underline{\sigma}}\right) = \rho\underline{b}. \tag{2.14}$$

2.2.3. Conservation of angular momentum. The angular momentum of the system is handled similarly to that of linear moment. We first formulate the global conservation law as the rate of change in angular momentum.

$$\begin{aligned}&\frac{\mathrm{d}}{\mathrm{d}t}\int_{\Omega_t} \underline{r}\times\left(\rho_s^*\left(1-\lambda\right)\underline{v}_s\right) + \underline{r}\times\left(\rho_f^*\lambda\underline{v}_f\right)\mathrm{d}\Omega \\ &= -\int_{\partial\Omega_t}\left(\left(\underline{r}\times\left(\rho_f^*\lambda\underline{v}_f\right)\right)\otimes\underline{w}_f\right)\underline{n}\mathrm{d}S \\ &\quad + \int_{\Omega_t}\underline{r}\times\rho\underline{b}\mathrm{d}\Omega \int_{\partial\Omega_t}\underline{r}\times\underline{t}\mathrm{d}S\end{aligned} \tag{2.15}$$

where in $\bar{r}$ is a spatial position vector for a material element of the homogenized mixture. Again, we have accounted for addition of angular momentum induced from relative fluid motion by the first term on the RHS. Using conservation of mass and linear momentum we obtain the local conservation of angular momentum equation which is a statement of symmetry of the Cauchy stress tensor for the combined medium.

$$\underline{\underline{\sigma}} - \underline{\underline{\sigma}}^T = 0. \tag{2.16}$$

2.3. Thermodynamic considerations

2.3.1. Energy and work rates. Now we determine the kinetic energy rate. Following the skeletal deformation and accounting for the additional kinetic energy due to relative fluid motion we have:

$$\begin{aligned}\frac{\mathrm{d}\overline{\mathcal{K}}}{\mathrm{d}t} &= \frac{1}{2}\frac{\mathrm{d}}{\mathrm{d}t}\int_{\Omega_t}\rho_s^*\left(1-\lambda\right)\underline{v}_s\cdot\underline{v}_s + \rho_f^*\lambda\underline{v}_f\cdot\underline{v}_f\mathrm{d}\Omega \\ &\quad + \frac{1}{2}\int_{\partial\Omega_t}\rho_f^*\lambda\left(\underline{v}_f\cdot\underline{v}_f\right)\left(\underline{w}_f\cdot\underline{n}_f\right)\mathrm{d}S \\ &= \int_{\Omega_t}\rho_s^*\left(1-\lambda\right)\underline{v}_s\cdot\underline{a}_s + \rho_f^*\lambda\underline{v}_f\cdot\underline{a}_f\mathrm{d}\Omega.\end{aligned} \tag{2.17}$$

Considering an external work rate skeletal deformation as well as an external work due to relative fluid motion we have the following energetic contributions [59].

$$\frac{\mathrm{d}W_{s,\,\mathrm{ext}}}{\mathrm{d}t} = \int_{\Omega_t} \rho \underline{b} \cdot \underline{v}_s \mathrm{d}\Omega + \int_{\partial\Omega_t} \underline{t} \cdot \underline{v}_s \mathrm{d}S \tag{2.18a}$$

$$\frac{\mathrm{d}W_{f,\mathrm{ext}}}{\mathrm{d}t} = \int_{\Omega_t} \lambda \rho_f^* \underline{b} \cdot \underline{w}_f \mathrm{d}\Omega + \int_{\partial\Omega_t} \lambda \underline{\underline{\sigma}}_f \underline{n} \cdot \underline{w}_f \mathrm{d}S \tag{2.18b}$$

where in we have introduced the fluid stress tensor $\underline{\underline{\sigma}}_f$ that may encompass hydrostatic pressure as well as viscous effects.

For the mobile species moving in the fluid phase, we consider the species of molar concentration c_β in moles per total volume and write the molar balance equation following the skeletal deformation.

$$\frac{\mathrm{d}}{\mathrm{d}t} \int_{\Omega_t} c_\beta \mathrm{d}\Omega = -\int_{\partial\Omega_t} c_\beta \underline{w}_\beta \cdot \underline{n} \mathrm{d}S. \tag{2.19}$$

This renders a local molar balance in terms of the filtration velocity or molar flux, $\underline{h}_\beta = c_\beta \underline{w}_\beta$, which characterizes the species movement relative to the skeletal phase due to effect such as diffusion, electromigration, and advection in a bulk medium.

$$\frac{\mathrm{d}c_\beta}{\mathrm{d}t} + c_\beta \,\mathrm{div}\left(\underline{v}_s\right) = -\mathrm{div}\left(\underline{h}_\beta\right). \tag{2.20}$$

The energy contribution due to these species is characterized through their chemical potentials μ_β and the work rate may be written as a function of the molar flux across a spatial surface moving with the skeleton [60].

$$\begin{aligned}\frac{\mathrm{d}W_\beta}{\mathrm{d}t} &= -\int_{\partial\Omega_t} \mu_\beta \underline{h}_\beta \cdot \underline{n} \mathrm{d}S \\ &= \int_{\Omega_t} \left(\frac{\partial c_\beta}{\partial t} + \mathrm{div}\left(c_\beta \underline{v}_s\right)\right)\mu_i - \underline{h}_\beta \cdot \mathrm{grad}\left(\mu_\beta\right)\mathrm{d}\Omega.\end{aligned} \tag{2.21}$$

To account for the electrical work, we take a similar approach as in [52] and begin by describing the electrical properties of the medium with electrostatics. In the realm of electrostatics, Maxwell's equations render the electric field, $\underline{e}$, curl-free, and hence is the gradient of a scalar potential function, i.e. the electric potential ϕ.

$$\mathrm{curl}\left(\underline{e}\right) = 0, \quad \underline{e} = -\mathrm{grad}\left(\phi\right). \tag{2.22}$$

The total volumetric charge ρ and surface charge ω are related to the electric displacement, $\underline{d}$, by the Gauss Law within the volume and the normal jump of the electric displacement along the boundary, respectively [61].

$$div\left(\underline{d}\right) = q, \;\; \|\underline{d} \cdot \underline{n}\| = \omega \tag{2.23}$$

We assume the charge in the system is made up of electrons, q_0, and charged (ionic) species γ, with concentrations c_γ and charge number z_γ. The total charge is then:

$$q = q_0 + \mathcal{F} \sum_\gamma z_\gamma c_\gamma \tag{2.24}$$

wherein $\mathcal{F}$ is Faraday's constant. The electronic work rate can now be defined, following the skeletal deformation, as shown below [61]. The right most integral is obtained after leveraging the definition of total charge and the divergence theorem across a jump discontinuity.

$$\begin{aligned}\frac{\mathrm{d}W_{\mathrm{elec}}}{\mathrm{d}t} &= \int_{\Omega_t} \phi \frac{\mathrm{d}}{\mathrm{d}t}\left(q_0 \mathrm{d}\Omega\right) + \int_{\partial\Omega_t} \phi \frac{\mathrm{d}}{\mathrm{d}t}\left(\omega \,\mathrm{d}S\right) \\ &= \int_{\Omega_t} \underline{e} \cdot \left(\frac{\partial d}{\partial t} + \mathrm{div}\left(\underline{d} \otimes \underline{v}_s\right) \right. \\ &\qquad \left. - \mathrm{grad}\left(\underline{v}_s\right)\underline{d}\right) - \mathcal{F}\phi \sum_\beta z_\beta \\ &\qquad \times \left(\frac{\partial c_\beta}{\partial t} + \mathrm{div}\left(c_\beta \underline{v}_s\right)\right)\mathrm{d}\Omega.\end{aligned} \tag{2.25}$$

Note that the spatial electric field and electric displacement are not directly power conjugate under a finite-strain framework for deformable materials [61, 62]. Further, the summation is taken across all fluid constituents (solvent and ions) when only the ionic species contribute to the work rate. The uncharged species have a charge number of zero ($z_\beta = 0$) and hence does not affect the work rate contribution.

The total internal energy is written in terms of an internal energy per mixture volume and is additive between the two phases. Hence, the internal energy rate can be written as

$$\begin{aligned}\frac{\mathrm{d}\bar{u}}{\mathrm{d}t} &= \frac{\mathrm{d}}{\mathrm{d}t}\int_{\Omega_t} u_s \mathrm{d}\Omega + \frac{\mathrm{d}_f}{\mathrm{d}t}\int_{\Omega_t} u_f \mathrm{d}\Omega \\ &= \int_{\Omega_t} \frac{\partial u}{\partial t} + \mathrm{div}\left(u_s \underline{v}_s\right) + \mathrm{div}\left(u_f \underline{v}_f\right)\mathrm{d}\Omega.\end{aligned} \tag{2.26}$$

Finally, we decompose the heat supply into a distributed volumetric supply as well as a heat flux.

$$Q = \int_{\Omega_t} r_q \mathrm{d}\Omega - \int_{\partial\Omega_t} \underline{h}_q \cdot \underline{n} \mathrm{d}S = \int_{\Omega_t} r_q - \mathrm{div}\left(\underline{h}_q\right)\mathrm{d}\Omega. \tag{2.27}$$

2.3.2. First and second laws of thermodynamics. The first law of thermodynamics states that the time rate of change in the total energy of the system, internal and kinetic, is equal to the rate of heat and external work supplied to the system.

$$\frac{\mathrm{d}\bar{u}}{\mathrm{d}t}+\frac{\mathrm{d}\overline{\mathcal{K}}}{\mathrm{d}t}=Q+\frac{\mathrm{d}W_{s,\,\mathrm{ext}}}{\mathrm{d}t}+\frac{\mathrm{d}W_{f,\,\mathrm{ext}}}{\mathrm{d}t}+\frac{\mathrm{d}W_{\mathrm{elec}}}{\mathrm{d}t}+\sum_{\beta}\frac{\mathrm{d}W_{\beta}}{\mathrm{d}t}. \tag{2.28}$$

We localize the energy balance equation by first assuming the fluid stress is spherical, accounting for the hydrostatic pressure, p, of the fluid phase such that $\underline{\underline{\sigma}}_f=-p\underline{\underline{I}}$. Additionally, we introduce the fluid internal energy, $\mathscr{u}_{f*}$, and enthalpy, $\mathscr{h}_{f*}$, per fluid mass, which are denoted by the addition of the subscripted star [58, 59].

$$\begin{aligned}\frac{\mathrm{d}u}{\mathrm{d}t}+u\,\mathrm{div}\left(\underline{v}_s\right)=&\,\underline{\underline{\sigma}}:\underline{\underline{D}}+\left(\underline{b}-\underline{a}_f\right)\cdot\underline{h}_f-\mathrm{div}\left(h_{f*}\underline{h}_f\right)\\&-\sum_{\beta}\underline{h}_{\beta}\cdot\mathrm{grad}\left(\mu_{\beta}\right)\\&+\sum_{\beta}\left(\mu_{\beta}-z_{\beta}\mathcal{F}\phi\right)\left(\frac{\partial c_{\beta}}{\partial t}+\mathrm{div}\left(c_{\beta}\underline{v}_s\right)\right)\\&+r_q-\mathrm{div}\left(\underline{h}_q\right)\\&+\underline{e}\cdot\left(\frac{\partial\underline{d}}{\partial t}+\mathrm{div}\left(\underline{d}\otimes\underline{v}_s\right)\right.\\&\left.-\mathrm{grad}\left(\underline{v}_s\right)\underline{d}\right).\end{aligned} \tag{2.29}$$

In the above, $\underline{\underline{D}}$ is the symmetric part of the spatial velocity gradient, known as the rate of deformation tensor. As with the internal energy, we write the total entropy as additive between the two phases and as a per mixture volume quantity. The entropy rate is then calculated as

$$\frac{\mathrm{d}\bar{s}}{\mathrm{d}t}=\int_{\Omega_t}\frac{\partial s}{\partial t}+\mathrm{div}\left(\mathscr{s}_s\underline{v}_s\right)+\mathrm{div}\left(\mathscr{s}_f\underline{v}_f\right)\mathrm{d}\Omega. \tag{2.30}$$

Now, the second law of thermodynamics states that the entropy production, the rate minus supply, must at all times be nonnegative. We relate the volumetric supply and flux of entropy to the volumetric supply and flux of heat through the thermodynamic temperature [63–65]. Forming the local entropy inequality, we obtain:

$$\begin{aligned}T\left(\frac{\partial s}{\partial t}+\mathrm{div}\left(s_s\underline{v}_s\right)+\mathrm{div}\left(s_f\underline{v}_f\right)\right)-\frac{\underline{h}_q}{T}\cdot\mathrm{grad}\left(T\right)\geq r_q\\-\mathrm{div}\left(\underline{h}_q\right).\end{aligned} \tag{2.31}$$

We combine the first law and second law equations to eliminate the heat sources and flux divergence terms on the right-hand side of the entropy inequality. In this process we introduce the fluid Gibbs free energy per fluid mass $\mathscr{g}_{f*}=\mathscr{u}_{f*}+\frac{p}{\rho_f^*}-T\mathscr{s}_{f*}$ as well as the Helmholtz free energy of the system $\psi=\mathscr{u}-T\mathscr{s}$ to finally obtain the spatial Clausius–Duhem inequality:

$$\begin{aligned}&\underline{\underline{\sigma}}:\underline{\underline{D}}-\mathscr{s}\frac{\mathrm{d}T}{\mathrm{d}t}-\left(\frac{\mathrm{d}\psi}{\mathrm{d}t}+\psi\,\mathrm{div}\left(\underline{v}_s\right)\right)\\&+\mathscr{g}_{f*}\left(\frac{\mathrm{d}\rho_f^*\lambda}{\mathrm{d}t}+\rho_f^*\lambda\,\mathrm{div}\left(\underline{v}_s\right)\right)\\&+\underline{e}\cdot\left(\frac{\partial\underline{d}}{\partial t}+\mathrm{div}\left(\underline{d}\otimes\underline{v}_s\right)-\mathrm{grad}\left(\underline{v}_s\right)\underline{d}\right)\\&+\sum_{\beta}\left(\mu_{\beta}-z_{\beta}\mathcal{F}\phi\right)\left(\frac{\partial c_{\beta}}{\partial t}+\mathrm{div}\left(c_{\beta}\underline{v}_s\right)\right)\\&-\sum_{\beta}\underline{h}_{\beta}\cdot\mathrm{grad}\left(\mu_{\beta}\right)-\frac{\underline{h}_q}{T}\cdot\mathrm{grad}\left(T\right)\\&+\frac{\underline{h}_f}{\rho_f^*}\cdot\left(\rho_f^*\left(\underline{b}-\underline{a}_f\right)-\mathrm{grad}\left(p\right)\right)\geq 0\end{aligned} \tag{2.32}$$

which can be transported into the material frame [58, 59]:

$$\begin{aligned}&\underline{\underline{S}}:\frac{\mathrm{d}\underline{\underline{E}}}{\mathrm{d}t}-\mathcal{S}\frac{\mathrm{d}T}{\mathrm{d}t}+g_{f*}\frac{\mathrm{d}\rho_f^*\Lambda}{\mathrm{d}t}+\underline{E}\cdot\frac{\mathrm{d}\underline{D}}{\mathrm{d}t}\\&+\sum_{\beta}\left(\mu_{\beta}-z_{\beta}\mathcal{F}\phi\right)\frac{\mathrm{d}C_{\beta}}{\mathrm{d}t}-\frac{\mathrm{d}\Psi}{\mathrm{d}t}\\&+\frac{\underline{H}_f}{\rho_f^*}\cdot\left(\rho_f^*\underline{\underline{F}}^T\left(\underline{b}-\underline{a}_f\right)-\mathrm{Grad}\left(p\right)\right)\\&-\sum_{\beta}\underline{H}_{\beta}\cdot\mathrm{Grad}\left(\mu_{\beta}\right)-\frac{\underline{H}_q}{T}\cdot\mathrm{Grad}\left(T\right)\geq 0\end{aligned} \tag{2.33}$$

wherein $\underline{\underline{S}}$ and $\underline{\underline{E}}$ are the 2nd Piola–Kirchhoff stress tensor and Green–Lagrange stain tensor, respectively. The Helmholtz free energy and entropy in the Lagrangian frame may be additively decomposed according to the free energy of the skeleton and the fluid, where we also write the fluid components in a per mass basis (i.e. $\Psi=\Psi_s+\rho_f^*\Lambda\psi_{f*}$, $\mathcal{S}=\mathcal{S}_s+\rho_f^*\Lambda\mathscr{s}_{f*}$). The Gibbs and Helmholtz free energies are related as $\psi_{f*}=\mathscr{g}_{f*}-\frac{p}{\rho_f^*}$, and noting that the Lagrangian representation of the fluid mass is written as $\rho_f^*\Lambda=\rho_f^*\lambda J$, we may further manipulate the inequality into the form below.

$$\underline{\underline{S}} : \frac{\mathrm{d}\underline{\underline{E}}}{\mathrm{d}t} - \not{s}_s \frac{\mathrm{d}T}{\mathrm{d}t} + p\frac{\mathrm{d}\Lambda}{\mathrm{d}t} + \underline{E}\cdot\frac{\mathrm{d}\underline{D}}{\mathrm{d}t} + \sum_\beta (\mu_\beta - z_\beta \mathcal{F}\phi)\frac{\mathrm{d}C_\beta}{\mathrm{d}t} - \frac{d\Psi_s}{\mathrm{d}t} - \sum_\beta \underline{H}_\beta \cdot \mathrm{Grad}\,(\mu_\beta) - \underline{H}_q \cdot \frac{\mathrm{Grad}\,(T)}{T} - \underline{H}_f \cdot \frac{\mathrm{Grad}\,(p)}{\rho_f^*} \geq 0. \tag{2.34}$$

Every quantity in equation (2.34) is written with reference to the skeletal phase. The effects of body forces, $\underline{b}$, and inertia, $\underline{a}_f$, on the relative fluid mass flux have been neglected for simplicity as they are expected to play a negligible role in the transduction behavior of the IPMC.

2.4. Membrane model closure and constitutive requirements

To close the model, we look at the saturation condition again. Recall that this condition requires the volume fractions (solid and fluid) add to unity.

$$\lambda_s + \lambda_f = 1. \tag{2.35}$$

We have already identified the fluid phase as being a miscible mixture of constituent species, and hence we may write the fluid volume fraction in terms of the constituent volume fractions. Further, we can identify the volume fractions of these constituent species in terms of their molar volumes, ν_i, and molar concentrations with respect to the combined medium, i.e.

$$\lambda_f = \sum_\beta \lambda_\beta, \quad \lambda_\beta = \nu_\beta c_\beta. \tag{2.36}$$

Combining this result with the saturation condition, accounting for $\lambda_s = 1 - \lambda$, we have a modified saturation condition which closes the model by connecting the membrane porosity to the chemical composition of the interstitial pore fluid through an ideal mixture of the constitute species. In the spatial and material frames, respectively, we have:

$$\lambda = \sum_\beta \nu_\beta c_\beta, \quad \Lambda = \sum_\beta \nu_\beta C_\beta. \tag{2.37}$$

The saturation condition may be enforced through a Lagrange multiplier, $\mathcal{P}$, and added to the entropy inequality in order to impose the constraint on the evolution of the system [57, 66–68]. The material time rate of the Lagrangian saturation condition is used in order to fit with the rate form of the Clasius–Duhem inequality.

$$\underline{\underline{S}} : \frac{\mathrm{d}\underline{\underline{E}}}{\mathrm{d}t} - \not{s}_s \frac{\mathrm{d}T}{\mathrm{d}t} + (p+\mathcal{P})\frac{\mathrm{d}\Lambda}{\mathrm{d}t} + \underline{E}\cdot\frac{\mathrm{d}\underline{D}}{\mathrm{d}t} + \sum_\beta (\mu_\beta - z_\beta\mathcal{F}\phi - \nu_\beta\mathcal{P})\frac{\mathrm{d}C_\beta}{\mathrm{d}t} - \frac{\mathrm{d}\Psi_s}{\mathrm{d}t} - \sum_\beta \underline{H}_\beta \cdot \mathrm{Grad}\,(\mu_\beta) - \underline{H}_q \cdot \frac{\mathrm{Grad}\,(T)}{T} - \underline{H}_f \cdot \frac{\mathrm{Grad}\,(p)}{\rho_f^*} \geq 0. \tag{2.38}$$

We find that the Lagrange multiplier manifests as an additional pressure term which modifies the fluid hydrostatic pressure, p, as well as introduces a pressure contribution to the chemical potential of the constituent species.

We now have the Clasius–Duhem inequality in a material description which is constrained by the saturation condition through a Lagrange multiplier. Next, we determine constitutive restrictions placed on the primary dependent fields. Following the Coleman-Noll procedure to formulate set of independent variables: $\underline{\underline{E}}$, T, J_s, $\underline{D}$, C_β [57, 60, 63, 64, 69]. The variable J_s is the local volumetric deformation of the solid constitute, J_s, and is used in place of the Lagrangian porosity Λ, as an independent variable with which the remaining fields vary [70].

$$J_s = \frac{\mathrm{d}\Omega_s}{\mathrm{d}\Omega_{s,0}} = \frac{1-\lambda}{1-\lambda_0} J. \tag{2.39}$$

With this set of variables, we obtain our final entropy inequality.

$$\left(\underline{\underline{S}} - \frac{\partial\Psi_s}{\partial\underline{\underline{E}}} + (p+\mathcal{P})J\underline{\underline{F}}^{-}\underline{\underline{F}}^{-T}\right) : \frac{d\underline{\underline{E}}}{\mathrm{d}t} - \left(\mathcal{S}_s + \frac{\partial\Psi_s}{\partial T}\right)\frac{dT}{\mathrm{d}t} - \left((1-\lambda_0)(p+\mathcal{P}) + \frac{\partial\Psi_s}{\partial J_s}\right)\frac{\mathrm{d}J_s}{\mathrm{d}t} + \left(\underline{E} - \frac{\partial\Psi_s}{\partial\underline{D}}\right)\cdot\frac{d\underline{D}}{\mathrm{d}t} + \sum_\beta \left(\mu_\beta - z_\beta\mathcal{F}\phi - \nu_\beta\mathcal{P} - \frac{\partial\Psi_s}{\partial C_\beta}\right)\frac{dC_\beta}{\mathrm{d}t} - \sum_\beta \underline{H}_\beta\cdot\mathrm{Grad}\,(\mu_\beta) - \underline{H}_q\cdot\frac{\mathrm{Grad}\,(T)}{T} - \underline{H}_f\cdot\frac{\mathrm{Grad}\,(p)}{\rho_f^*} \geq 0. \tag{2.40}$$

We see that the transition from the material frame porosity to the local solid constituent volume deformation has combine the pressure contributions with the stress tensor which is a manifestation of Terzaghi's Principle of soil mechanics [65, 71], where the 2nd Piola–Kirchhoff stress represents the effective stress, i.e. the difference between the total stress and combined pressure (hydrostatic pressure and Lagrange multiplier).

For this inequality to represent a thermodynamically consistent processes, it must hold for all arbitrarily chosen values for the material derivatives of $\underline{\underline{E}}$, T, J_s, $\underline{D}$, C_β. The parenthetical expressions are not functionally dependent on the rate terms they multiply, and hence they must equate to zero for an arbitrary assignment of the time rate fields.

$$\begin{aligned}
\underline{\underline{S}} &= \frac{\partial\Psi_s}{\partial\underline{\underline{E}}} - \not{J}\underline{\underline{F}}^{-}\underline{\underline{F}}^{-T}, \quad \not{} = -\frac{1}{1-\lambda_0}\frac{\partial\Psi_s}{\partial J_s} \\
\mathcal{S}_s &= -\frac{\partial\Psi_s}{\partial T}, \quad \mu_\beta = \frac{\partial\Psi_s}{\partial C_\beta} + z_\beta\mathcal{F}\phi + \nu_\beta\mathcal{P}, \\
\underline{E} &= \frac{\partial\Psi_s}{\partial\underline{D}} = -\mathrm{Grad}\,(\phi).
\end{aligned} \tag{2.41}$$

Here we have combined the hydrostatic pressure with the Lagrange multiplier to obtain a unified pressure, $\mathscr{p} = p + \mathcal{P}$, referred to hereon as the conjugate pressure (i.e. the pressure which is power conjugate to the solid constituent volume deformation). The pressure contribution from the Lagrange multiplier will be referred to as the Lagrange pressure.

We allow every flux term to vary linearly with all other thermodynamic driving forces:

$$\underline{H}_i = -\sum_j \underline{\underline{M}}_{ij}\underline{F}_j. \tag{2.42}$$

The Onsager coefficients, $\underline{\underline{M}}_{ij}$, are written as rank-2 tensors (mobility tensors) to allow for the possibility of anisotropic transport, this formulation then satisfies the remaining entropy inequality so long as the matrix of mobility tensors $\left[\underline{\underline{M}}_{ij}\right]$ is positive-semidefinite [60].

$$\left[\underline{\underline{M}}_{ij}\right] = \begin{bmatrix} \underline{\underline{M}}_{11} & \underline{\underline{M}}_{12} & \cdots & \underline{\underline{M}}_{1N} \\ \underline{\underline{M}}_{21} & \underline{\underline{M}}_{22} & \cdots & \underline{\underline{M}}_{2N} \\ \vdots & \vdots & \ddots & \vdots \\ \underline{\underline{M}}_{N1} & \underline{\underline{M}}_{N2} & \cdots & \underline{\underline{M}}_{NN} \end{bmatrix}, \left[\underline{\underline{M}}_{ij}\right] : \underline{x}^T \left[\underline{\underline{M}}_{ij}\right] \underline{x} \geq 0 \forall \underline{x}. \tag{2.43}$$

We further enforce that this matrix of mobilities follows the Onsager reciprocal relations, thereby rendering the matrix symmetric [72, 73].

2.5. The electrode domain and interface coupling under finite deformation

As opposed to the multiphasic continua that makes up the polymer membrane, we treat the electrode as a single homogenous conductive material that deforms along with the solid skeleton. This, in effect, allows for the same mechanical conservation laws (mass and momentum) to hold upon setting $\lambda = 0$ (no fluid permeation into the electrode domain), along with appropriate material properties.

As for the electrical properties in this domain, we could treat the electrodes as perfect conductors which is typical for finite-strain formulations [36, 46, 74]. Including resistive effects requires more care in the coupling between electrode and polymer domains. The electrical and ionic currents may be related through the Ramo–Shockley theorem or Gauss's Law [48, 75, 76], but here we develop a new framework for coupling the electrode and polymer domains using the notation of interfacial charge conservation. Of importance is this new framework is valid under a finite-strain formulation and recovers the previous electrode couplings obtained by Ramo-Shockley or Gauss's Law arguments under a single conservation law equation.

2.5.1. Lossy electrode field equations. We again work under the assumption of electrostatics, that is, a curl-free electric field. We furthermore may invoke the classical jump conditions of electrostatics for these fields. For an imperfect electrode, one with finite electrical conductivity, we account for resistive losses using the differential form of Ohm's law [46, 75, 77–82]. We have the Eulerian and Lagrangian representation of Ohm's law below.

$$\underline{e} = \underline{\underline{r}}_e \underline{j}_e, \quad \underline{E} = \underline{\underline{R}}_e \underline{J}_e \tag{2.44}$$

wherein $\underline{\underline{r}}_e$ ($\underline{\underline{R}}_e$) is the spatial (material) electrical resistivity tensor and $\underline{j}_e$ ($\underline{J}_e$) is the spatial (material) electric current density in the electrode.

With differential Ohm's law, one could further propose a functional relationship between the electrical resistivity and the state of deformation within the electrode domain, i.e. $\underline{\underline{r}}_e := \underline{\underline{r}}_e\left(\underline{\underline{F}}\right)$. This would allow one to capture variable resistance due to the nano- and micro-structure of the conducive particles as they are composited with the membrane [82, 83]. Furthermore, the type of electroding material dictates the resistivity and structure of the electrodes which have marked effects on the behavior of the IPMC [84–86].

As we are relating the electric field to the current density in the electrode domain via Ohm's law, we also require a relation for charge conservation at an interface in order to couple the ionic and displacement currents in the IPMC membrane with the electronic currents inside the electrode domains. This formulation supersedes the jump conditions in terms of the polymer-electrode interface coupling.

2.5.2. Charge conservation at a deforming material interface. We start with the formulation of interfacial charge conservation and consider a control volume V such that the surfaces of this volume within media 1 and 2 follow the topology of the interface S. We let the height separating these two surfaces tend toward zero and hence the volume contained in this space vanishes, and the normal to surface A matches the normal to surface S, see figure 3 [87].

Within this control volume, we have the following conservation law for the interfacial charge [87].

$$\int_A \left\| \underline{j} \cdot \underline{n}_S \right\| \mathrm{d}S + \oint_C \underline{i}^S \cdot \underline{n}_C \mathrm{d}\ell = -\frac{d}{dt}\int_A \mathscr{w}\, \mathrm{dS} \tag{2.45}$$

Forming an orthonormal basis using the surface normal $\underline{n}_S$, curve normal $\underline{n}_C$, and curve tangent $\underline{t}_C$ and reparametrize the second integrand on the left-hand-side (LHS) of equation (2.45) we obtain the following.

$$\int_A \left\| \underline{j} \cdot \underline{n}_S \right\| \mathrm{d}S + \oint_C \left(\underline{n}_S \times \underline{i}^S\right) \cdot \left(\underline{t}_C \mathrm{d}\ell\right) = -\frac{d}{dt}\int_A \mathscr{w}\, \mathrm{dS} \tag{2.46}$$

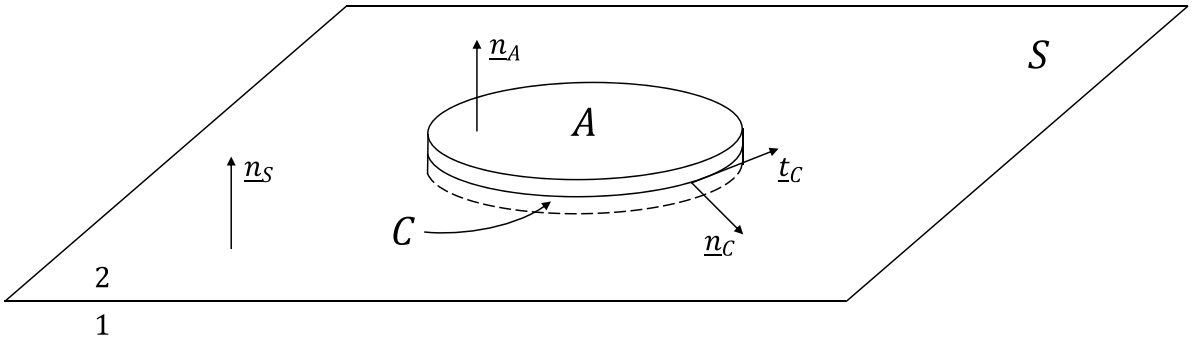

Figure 3. Schematic of interfacial charge conservation. Recreated from [87]. The interface surface $\boldsymbol{S}$ is intersected by a control volume whose thickness approaches zero, leaving a surface area $\boldsymbol{A}$ on either side of the interface. The volume intersects the surface along a contour $\boldsymbol{C}$. Normal and tangential vectors for the surface, area, and contour are provided.

Next, we leverage Stokes' theorem to transform the path integral into a surface integral and recast the resulting curl operator to obtain [88]:

$$\int_A \left\|\underline{j}\cdot\underline{n}\right\| \mathrm{d}S + \int_A div_S\left(\underline{i}^S\right) + 2H\left(\underline{i}^S\cdot\underline{n}\right)\mathrm{d}S = -\frac{d}{dt}\int_A \omega\ \mathrm{dS} \tag{2.47}$$

Here we dropped the subscript on the surface normal (i.e. $\underline{n}_S = \underline{n}$) and have introduced the surface divergence, $\mathrm{div}_s(\square)$, and mean curvature, H, defined below using the spatial surface projection tensor, $\underline{\underline{\mathbb{p}}}$ [89–91].

$$\underline{\underline{\mathbb{p}}} = \underline{\underline{I}} - \underline{n}\otimes\underline{n} \tag{2.48a}$$

$$\mathrm{div}_s(\square) = \mathrm{tr}\left(\mathrm{grad}(\square)\,\underline{\underline{\mathbb{p}}}\right) \tag{2.48b}$$

$$H = -\frac{1}{2}\mathrm{div}_S\left(\underline{n}_S\right). \tag{2.48c}$$

Since the surface current density is a tangential surface vector, i.e. has no normal component, the second integral on the LHS retains only the surface divergence term and we are left with the following.

$$\int_A \left\|\underline{j}\cdot\underline{n}\right\| \mathrm{d}S + \int_A div_S\left(\underline{i}^S\right)\mathrm{d}S = -\frac{d}{dt}\int_A \omega\ \mathrm{d}S \tag{2.49}$$

This result is in alignment with the surface divergence theorem, or surface Green's theorem [89, 90, 92], for tangential vectors, and recovers the final conservation law in [87] using purely calculus based arguments and an explicit definition of the surface divergence. To deal with the right-most term we use the transport relations for interfacial fields on material surfaces [92, 93] to obtain the integral and differential forms of charge conservation at a material surface under finite-strains in the Eulerian form:

$$\int_A \left\|\underline{j}\cdot\underline{n}\right\| + \mathrm{div}_S\left(\underline{i}^S\right)\mathrm{d}S = -\int_A \frac{d\omega}{dt} + \omega\ \mathrm{div}_S(\underline{v})\,\mathrm{d}S \tag{2.50a}$$

$$div_S\left(\underline{i}^S\right) + \left\|\underline{j}\cdot\underline{n}\right\| = -\left(\frac{dw}{dt} + \omega\ \mathrm{div}_S(\underline{v})\right) \tag{2.50b}$$

and Lagrangian form:

$$\int_{A_0} \|\underline{J}\cdot\underline{N}\| + J\left|\underline{\underline{F}}^{-T}\underline{N}\right| \mathrm{Div}_S\left(\underline{\underline{F}}^{-T}\underline{I}^S\right)\mathrm{d}S_0 = -\int_{A_0}\frac{d\mathcal{W}}{dt}\mathrm{d}S_0 \tag{2.51a}$$

$$J\left|\underline{\underline{F}}^{-T}\underline{N}\right| \mathrm{Div}_S\left(\underline{\underline{F}}^{-T}\underline{I}^S\right) + \|\underline{J}\cdot\underline{N}\| = -\frac{d\mathcal{W}}{dt} \tag{2.51b}$$

wherein we have introduced the material surface charge density, surface current density, surface divergence, and surface projection tensor defined below.

$$\mathcal{W}\,\mathrm{d}S_0 = \omega\,\mathrm{d}S,\ \underline{I}^S\mathrm{d}\ell_0 = \underline{i}^S\mathrm{d}\ell \tag{2.52a}$$

$$\mathrm{Div}_S(\square) = \mathrm{tr}\left(\underline{\underline{F}}^{-T}\mathrm{Grad}(\square)\,\underline{\underline{\mathbb{P}}}\right),\quad \underline{\underline{\mathbb{P}}} = \underline{\underline{I}} - \left(\underline{\underline{F}}^{-T}\underline{N}\right)\otimes\left(\underline{\underline{F}}^{-T}\underline{N}\right). \tag{2.52b}$$

3. Governing equations for the IPMC

3.1. Helmholtz thermodynamic potential

To develop an initial model for the IPMC membrane under the newly derived porous media framework we use an additive decomposition of the skeletal free energy with mechanical, ionic, solvent, polarization, and volumetric components [33, 34, 94–96].

$$\Psi_s = \Psi_{\mathrm{mech}} + \Psi_{\mathrm{ion}} + \Psi_{\mathrm{solv}} + \Psi_{\mathrm{pol}} + \Psi_{\mathrm{vol}} \tag{3.1a}$$

$$\Psi_{\text{mech}} = \frac{\mathcal{C}_\lambda}{2} tr\left(\underline{\underline{E}}\right)^2 + \mathcal{C}_\mu tr\left(\underline{\underline{E}}^2\right) \tag{3.1b}$$

$$\Psi_{\text{ion}} = RT\left(C_+\left(\ln\left(\frac{C_+}{JC_{+,0}}\right) - 1\right) - C_{+,0}\left(\ln\left(\frac{1}{J}\right) - 1\right)\right) \tag{3.1c}$$

$$\Psi_{\text{solv}} = RT\left(C_w\left(\ln\left(\frac{C_w}{JC_{w,0}}\right) - 1\right) - C_{w,0}\left(\ln\left(\frac{1}{J}\right) - 1\right)\right) \tag{3.1d}$$

$$\Psi_{\text{pol}} = \frac{1}{2\in}\frac{\left(\underline{\underline{F}}^T\underline{\underline{F}}\right) : \left(\bar{D}\otimes\bar{D}\right)}{J} \tag{3.1e}$$

$$\Psi_{\text{vol}} = \mathcal{C}_K\left(J_s - 1 - \ln\left(J_s\right)\right). \tag{3.1f}$$

The mechanical contribution corresponds to a Saint Venant–Kirchhoff material model [97]. We have included the entropy contributions of the mobile cation species C_+ with initial concentration $C_{+,0}$ as well as the solvent water, with concentration C_w and initial concentration $C_{w,0}$. These terms represent the entropic contributions of each species independently as opposed to the entropy of mixing for the combine solution [56], and the coupling of these species is made through the flux relations and saturation condition. The polarization component models an ideal, linear dielectric material. Lastly, we have included a classical form for the volumetric contribution to the free energy [59], wherein the bulk modulus $\mathcal{C}_K$ can be written in terms of the Lamé moduli, $\mathcal{C}_\lambda$ and $\mathcal{C}_\mu$, as $\mathcal{C}_K = \mathcal{C}_\lambda + \frac{2}{3}\mathcal{C}_\mu$.

3.2. Field equations in the material frame

With this definition for the thermodynamic free energy, we can derive the 2nd Piola–Kirchhoff stress according to our constitutive equations.

$$\begin{aligned}\underline{\underline{S}} = {} & \mathcal{C}_\lambda tr\left(\underline{\underline{E}}\right)\hat{I} + 2\mathcal{C}_\mu\underline{\underline{E}} + \underline{\underline{F}}^{-1}\underline{\underline{F}}^{-T}RT(C_{+,0} - C_+ + C_{w,0} - C_w) \\ & + \frac{1}{2\in}\underline{\underline{F}}^{-1}\left(\frac{2\underline{\underline{F}}\left(\underline{\underline{D}}\otimes\underline{\underline{D}}\right)}{J} - \frac{\left(\underline{\underline{FD}}\right)\cdot\left(\underline{\underline{FD}}\right)}{J}\underline{\underline{F}}^{-T}\right) \\ & - pJ\underline{\underline{F}}^{-1}\underline{\underline{F}}^{-T}.\end{aligned} \tag{3.2}$$

Note that the inclusion of the solvent species introduces an additional osmotic pressure not found in the IPMC models found in literature, and we find a Maxwell stress contribution due to polarization effects [33, 34]. The conjugate pressure, included in the stress above, is calculated from changes in solid volume deformation and material frame porosity below. The linearized form of this equation is similar to what has been considered for the fluid pressure in [75], wherein the p-wave modulus was used in place of the bulk modulus and membrane porosity is neglected.

$$p = -\frac{\mathcal{C}_K}{J-\Lambda}\left(\frac{J-\Lambda}{1-\lambda_0} - 1\right). \tag{3.3}$$

In the Lagrangian description, the balance of linear momentum, with no body forces and neglecting the fluid inertia, is rendered below.

$$\rho^*_{s,0}\left(1-\lambda_0\right)\underline{a}_s = \text{Div}\left(\underline{\underline{FS}}\right). \tag{3.4}$$

Similarly, the electrostatic equations may be written as:

$$\text{Div}\left(\underline{D}\right) = \mathcal{F}\sum_i z_i C_i, \quad \underline{E} = \frac{1}{\in}\frac{\underline{\underline{F}}^T\underline{\underline{FD}}}{J} = -\text{Grad}\left(\phi\right). \tag{3.5}$$

The fixed anions vary according to the volumetric strain of the medium in the Eulerian description [33, 75, 81].

$$c_- = \frac{c_{-,0}}{1+\varepsilon_V}, \quad \varepsilon_V = J - 1. \tag{3.6}$$

This effect is commonly neglected in actuation models, and therein the anions take on a fixed initial concentration $c_- = c_{-,0}$. In the material frame the anion species simply remains constant at its initial concentration. Here we consider isothermal conditions and hence ignore the thermal gradient and its flux coupling in the model. Furthermore, neglecting the inertial effects of the fluid phase and assuming no body forces, we couple the cation and solvent water flux to each other along with the mechanical contribution to the fluid velocity and obtain:

$$\underline{H}_+ = -\underline{\underline{M}}_{++}\text{Grad}\left(\mu_+\right) - \underline{\underline{M}}_{+w}\text{Grad}\left(\mu_w\right) - \underline{\underline{M}}_{+f}\text{Grad}\left(p\right) \tag{3.7a}$$

$$\underline{H}_w = -\underline{\underline{M}}_{w+}\text{Grad}\left(\mu_+\right) - \underline{\underline{M}}_{ww}\text{Grad}\left(\mu_w\right) - \underline{\underline{M}}_{wf}\text{Grad}\left(p\right) \tag{3.7b}$$

$$\frac{\underline{H}_f}{\rho^*_f} = -\underline{\underline{M}}_{f+}\text{Grad}\left(\mu_+\right) - \underline{\underline{M}}_{fw}\text{Grad}\left(\mu_w\right) - \underline{\underline{M}}_{ff}\text{Grad}\left(p\right). \tag{3.7c}$$

The chemical potentials of the constituent fluid species, and their material gradients are given below, wherein we assume the initial concentration fields are spatially uniform.

$$\mu_+ = RT\ln\left(\frac{C_+}{JC_0}\right) + z_+\mathcal{F}\phi + \nu_+\mathcal{P} \tag{3.8a}$$

$$\text{Grad}\left(\mu_+\right) = J\frac{RT}{C_+}\text{Grad}\left(\frac{C_+}{J}\right) + z_+\mathcal{F}\text{Grad}\left(\phi\right) + \nu_+\text{Grad}\left(\mathcal{P}\right) \tag{3.8b}$$

$$\mu_w = RT\ln\left(\frac{C_w}{JC_{w,0}}\right) + \nu_w\mathcal{P} \tag{3.8c}$$

$$\text{Grad}\,(\mu_w) = J\frac{RT}{C_w}\text{Grad}\left(\frac{C_w}{J}\right) + \nu_w\text{Grad}\,(\mathcal{P})\,. \tag{3.8d}$$

Also note that we have an additional equation defining the hydrostatic pressure in terms of the Lagrange and conjugate pressures $p = p - \mathcal{P}$.

To identity the material frame Onsager coefficients used in equation (3.7) we first start in the spatial frame and write the matrix of coefficients, assuming isotropic mobility, as

$$\begin{aligned}[m_{ij}] &= \begin{bmatrix} m_{++} & m_{+w} & m_{+f} \\ m_{w+} & m_{ww} & m_{wf} \\ m_{f+} & m_{fw} & m_{ff} \end{bmatrix} \\ &= \begin{bmatrix} \dfrac{\mathcal{D}_{++}c_+}{RT} & \dfrac{\mathcal{D}_{+w}c_w}{RT} & k_f c_+ \\ \dfrac{\mathcal{D}_{w+}c_+}{RT} & \dfrac{\mathcal{D}_{ww}c_w}{RT} & k_f c_w \\ k_f c_+ & k_f c_w & k_f\lambda \end{bmatrix} \end{aligned} \tag{3.9}$$

wherein $\mathcal{D}_{ij}$ is the diffusivity of species i with respect to the species j, k_f is the hydraulic permeability, taken as a constant. With the matrix defined in the spatial frame, a simple pull-back operation gives the material frame representation of each mobility term.

$$\begin{aligned}[M_{ij}] &= J\underline{\underline{F}}^{-}\,[m_{ij}]\,\underline{\underline{F}}^{-T} \\ &= \underline{\underline{F}}^{-}\underline{\underline{F}}^{-T}\begin{bmatrix} \dfrac{\mathcal{D}_{++}C_+}{RT} & \dfrac{\mathcal{D}_{+w}C_w}{RT} & k_f C_+ \\ \dfrac{\mathcal{D}_{w+}C_+}{RT} & \dfrac{\mathcal{D}_{ww}C_w}{RT} & k_f C_w \\ k_f C_+ & k_f C_w & Jk_f\lambda \end{bmatrix}. \end{aligned} \tag{3.10}$$

Note that pull-back operation above acts on matrix $[m_{ij}]$ elementwise. We can now write the flux of each constituent fluid species and bulk fluid in the material frame.

$$\begin{aligned}\underline{H}_+ = -\underline{\underline{F}}^{-}\underline{\underline{F}}^{-T}\mathcal{D}_{++}\Big(&J\,\text{Grad}\left(\frac{C_+}{J}\right) \\ &+ \frac{z_+\mathcal{F}C_+}{RT}\text{Grad}\,(\phi) + \frac{\nu_+C_+}{RT}\text{Grad}\,(P) \\ &+ \frac{\mathcal{D}_{+w}}{\mathcal{D}_{++}}\left(J\,\text{Grad}\left(\frac{C_w}{J}\right) + \frac{\nu_w C_w}{RT}\text{Grad}\,(P)\right) \\ &+ \frac{k_f C_+}{\mathcal{D}_{++}}\text{Grad}\,(p)\Big)\end{aligned} \tag{3.11a}$$

$$\begin{aligned}\underline{H}_w = -\underline{\underline{F}}^{-}\underline{\underline{F}}^{-T}\mathcal{D}_{w+}\Big(&J\,\text{Grad}\left(\frac{C_+}{J}\right) \\ &+ \frac{z_+\mathcal{F}C_+}{RT}\text{Grad}\,(\phi) + \frac{\nu_+C_+}{RT}\text{Grad}\,(P) \\ &+ \frac{\mathcal{D}_{ww}}{\mathcal{D}_{w+}}\left(J\,\text{Grad}\left(\frac{C_w}{J}\right) + \frac{\nu_w C_w}{RT}\text{Grad}\,(P)\right) \\ &+ \frac{k_f C_w}{\mathcal{D}_{w+}}\text{Grad}\,(p)\Big)\end{aligned} \tag{3.11b}$$

$$\begin{aligned}\frac{\underline{H}_f}{\rho_f^*} = -\underline{\underline{F}}^{-}\underline{\underline{F}}^{-T}k_f(&\Lambda\text{Grad}\,(p) + RT\,\text{Grad}\,(C_+ + C_w) \\ &- RT\,(C_+ + C_w)\,\text{Grad}\,(\ln(J)) + z_+C_+\mathcal{F}\text{Grad}\,(\phi)).\end{aligned} \tag{3.11c}$$

3.2.1. Thermodynamic restrictions on the matrix of mobility tensors. We must ensure that the matrix of mobilities is positive-semidefinite. Firstly, we enforce that the matrix be symmetric, following the Onsager relations, and hence can use the modified Sylvester's criterion to establish the requirements for a positive-semidefinite matrix. The modified Sylvester's criterion requires all principal minors of matrix $[m_{ij}]$ be nonnegative [98]. For symmetry we may simply enforce the following definition for the cross-diffusivity coefficient.

$$\mathcal{D}_{+w} = \mathcal{D}_{w+}\frac{c_+}{c_w}. \tag{3.12}$$

These cross-diffusivity terms may be characterized through the drag coefficient of water and the drag coefficient of the cation [21, 43], defined by

$$n_{dw} = \frac{\mathcal{D}_{w+}}{\mathcal{D}_{++}}, \quad n_{d+} = \frac{\mathcal{D}_{+w}}{\mathcal{D}_{ww}} = \frac{\mathcal{D}_{++}}{\mathcal{D}_{ww}}\frac{c_+}{c_w}n_{dw}. \tag{3.13}$$

The requirement of a positive-semidefinite according to the modified Sylvester's criterion gives us four inequalities that must be satisfied.

$$n_{dw}n_{d+} \leq 1 \tag{3.14a}$$

$$k_f \leq \frac{\lambda}{RT}\frac{\mathcal{D}_{++}}{c_+} \tag{3.14b}$$

$$k_f \leq \frac{\lambda}{RT}\frac{\mathcal{D}_{ww}}{c_w} \tag{3.14c}$$

$$\left(\frac{c_w}{c_+} + \frac{\mathcal{D}_{ww}}{\mathcal{D}_{++}} - 2n_{dw}\right)k_f \leq \frac{\lambda}{RT}\frac{\mathcal{D}_{ww}}{c_+}\,(1 - n_{dw}n_{d+})\,. \tag{3.14d}$$

The first of which aligns with that found in [43], which accounted only for the cross diffusion of the solvent and mobile ions and not of the bulk fluid transport. The remaining three inequalities may be used to construct estimates for the maximum hydraulic permeability allowable under limiting scenarios such as complete ionic depletion and infinite ionic concentration. A positive-semidefinite mobility matrix in the spatial frame guarantees that the matrix in the material frame matrix will also be positive-semidefinite and thus we have fully accounted for the thermodynamic restrictions on the model.

3.2.2. Dynamic drag coefficients and the hydraulic permeability. As discussed in [43], equation (3.14*a*) indicates that a modification of the water and cation drag coefficients is necessary when the concentration ratio of solvent to ions exceeds a certain critical value. Here we present an alternative expression for the dynamic drag coefficients which is continuous as the critical value is crossed, as opposed to the jump discontinuity found in [43].

$$n'_{d+} = \begin{cases} \dfrac{1}{n_{dw}} & \dfrac{c_+}{c_w} > \frac{1}{\gamma} \\ \dfrac{\mathcal{D}_+ c_+}{\mathcal{D}_w c_w} n_{dw} & \dfrac{c_+}{c_w} \leq \frac{1}{\gamma} \end{cases}, \qquad n\prime_{dw} = \begin{cases} \dfrac{\mathcal{D}_w c_w}{\mathcal{D}_+ c_+} \dfrac{1}{n_{dw}} & \dfrac{c_+}{c_w} > \dfrac{1}{\gamma} \\ n_{dw} & \dfrac{c_+}{c_w} \leq \frac{1}{\gamma} \end{cases}. \tag{3.15}$$

These replace the drag coefficients in the previous analysis, with all thermodynamic inequalities being the same. The parameter γ is a measure of the solvent to cation concentration ratio whereby a change in drag coefficients is necessary as per the thermodynamic requirements.

$$\gamma = \frac{\mathcal{D}_+}{\mathcal{D}_w} n_{dw}^2. \tag{3.16}$$

3.3. Kinematic linearization of the field equations

Now we linearize these equations under a small displacement assumption, wherein the spatial and material frames coincide, and we can write $\underline{X} = \underline{x}$ and use the nabla form of the differential operators. The deformation gradient tensor and its Jacobian is linearized to $\underline{\underline{F}} \approx \underline{\underline{I}}$ and $J \approx 1$, respectively, for most of the model. Regarding the pressure contributions, we approximate the deformation gradient Jacobian as

$$J \approx 1 + \nabla \cdot \underline{u} \tag{3.17}$$

which allows one to retain the effects of deformation on the convective flux for the ionic and solvent species. The Green-Lagrange strain tensor linearizes to the infinitesimal strain tensor:

$$\underline{\underline{E}} \approx \underline{\underline{\varepsilon}} = \frac{1}{2}\left(\nabla \underline{u} + (\nabla \underline{u})^T\right). \tag{3.18}$$

Under this scheme the stress, equilibrium, and electrostatic equations are fully defined below.

$$\underline{\underline{\sigma}} = \mathcal{C}_\lambda tr\left(\underline{\underline{\varepsilon}}\right)\underline{\underline{I}} + 2\mathcal{C}_\mu \underline{\underline{\varepsilon}} + RT(c_{+,0} - c_+ + c_{w,0} - c_w)\underline{\underline{I}} + \frac{1}{\in}\left(\underline{d}\otimes\underline{d} - \frac{1}{2}(\underline{d}\cdot\underline{d})\underline{\underline{I}}\right) - p\underline{\underline{I}} \tag{3.19a}$$

$$p = -\frac{\mathcal{C}_K}{1-\lambda}\left(\frac{\lambda_0 - \lambda}{1-\lambda_0} + \nabla \cdot \underline{u}\right) \tag{3.19b}$$

$$\rho^*_{s,0}(1-\lambda_0)\frac{d^2\underline{u}}{dt^2} = \nabla \cdot \underline{\underline{\sigma}}^T \tag{3.19c}$$

$$\nabla \cdot \underline{d} = \mathcal{F}(z_+ c_+ + z_- c_-) \tag{3.19d}$$

$$\underline{d} = -\in \nabla\phi. \tag{3.19e}$$

The cation and solvent chemical potentials and their gradients similarly linearize, and we may use the spatial representation of the Onsager coefficients given in equations (3.9) to write the ionic, solvent water, and relative fluid mass fluxes.

$$\underline{h}_+ = -\mathcal{D}_{++}\left(\nabla c_+ + \frac{z_+\mathcal{F}c_+}{RT}\nabla\phi + \frac{\nu_+ c_+}{RT}\nabla P\right) - \mathcal{D}_{ww} n_{d+}\left(\nabla c_w + \frac{\nu_w c_w}{RT}\nabla P\right) + c_+ \underline{w}_f{}^m \tag{3.20a}$$

$$\underline{h}_w = -n_{dw}\mathcal{D}_{++}\left(\nabla c_+ + \frac{z_+\mathcal{F}c_+}{RT}\nabla\phi + \frac{\nu_+ c_+}{RT}\nabla P\right) - \mathcal{D}_{ww}\left(\nabla c_w + \frac{\nu_w c_w}{RT}\nabla P\right) + c_w \underline{w}_f{}^m \tag{3.20b}$$

$$\underline{h}_f = -\rho^*_f k_f(\lambda\nabla p + z_+\mathcal{F}c_+\nabla\phi + RT(\nabla c_+ + \nabla c_w) + \lambda\nabla P). \tag{3.20c}$$

We can see that the ionic flux will render an augmented-PNP system that accounts for the solvent drag effects and bulk fluid motion. The third equation above can be rewritten in terms of the filtration velocity and takes the form of a modified Darcy's law.

$$\lambda\underline{w}_f = -k_f(\lambda\nabla p + z_+\mathcal{F}c_+\nabla\phi + RT\nabla(c_+ + c_w) + \lambda\nabla P) = \lambda\left(\underline{w}_f{}^m + \underline{w}_f{}^e + \underline{w}_f{}^c + \underline{w}_f^{sat}\right) \tag{3.21a}$$

$$\underline{w}_f{}^m = -k_f\nabla p,\ \underline{w}_f{}^e = -\frac{k_f}{\lambda}z_+\mathcal{F}c_+\nabla\phi$$

$$\underline{w}_f{}^c = -\frac{k_f}{\lambda}RT\nabla(c_+ + c_w),\ \underline{w}_f^{\text{sat}} = -k_f\nabla P. \tag{3.21b}$$

The fields $\underline{w}_f{}^m$, $\underline{w}_f{}^e$, $\underline{w}_f{}^c$, and $\underline{w}_f^{\text{sat}}$ are the mechanical, electrical, concentration, and saturation contributions to the Darcy velocity [99]. We see that the cation and solvent fluxes take the form of coupled Nernst–Planck equations with convection in a bulk fluid, while the fluid velocity is a modified form of Darcy's law with mechanical, electroosmotic, osmotic, and fluid saturation effects.

3.4. Superficial electrode model

For the electrode domain, we proceed with the notion of a superficial electrode (one of zero thickness). Using the surface form of differential Ohm's law, which relates the tangential electric $\underline{e}_t$ to the surface current density $\underline{i}^S$ through the surface resistivity $\underline{\underline{r}}_e^S$. The tangential electric field is the surface gradient of the electric potential along the electrode, defined below.

$$\underline{e}_t = \underline{\underline{r}}_e^S \underline{i}^S,\ \underline{e}_t = -\nabla_S \phi \tag{3.22a}$$

$$\nabla_S(\square) = \nabla(\square) - \underline{n}(\underline{n}\cdot\nabla(\square)). \tag{3.22b}$$

For the superficial electrode the electric current density inside the electrode domain is zero, and we only retain the surface current density. Hence, under the linearized framework the interfacial charge conservation allows us to relate the surface current density to the normal current density inside the polymer.

$$\nabla_S \cdot \underline{i}^S = \underline{i}\cdot\underline{n}, \underline{i} = -\frac{\partial}{\partial t}(\in \nabla\phi) + z_+ \mathcal{F} \underline{h}_+. \tag{3.23}$$

Accounting for ion-blocking electrodes, we can formulate the governing equation for the electric potential along the polymer-electrode interface.

$$-\nabla_S \cdot \left(\underline{\underline{\sigma}}_e^S \nabla_S \phi\right) = -\in \frac{\partial}{\partial t}(\nabla\phi\cdot\underline{n}) \tag{3.24}$$

wherein $\underline{\underline{\sigma}}_e^S$ is the surface electrical conductivity tensor, which is the inverse of the surface resistivity. We consider the free end of the IPMC as open circuited, i.e. no surface currents.

$$\overline{i}^S|_{x=L} = 0, \nabla_S\phi|_{x=L} = 0. \tag{3.25}$$

Additionally, a portion of the IPMC boundary is in electrical contact with an external circuit which delivers the applied voltage source for actuation and the open-circuit voltage or closed-circuit current signal is obtained during sensing. For an applied voltage, we may write

$$\phi = \phi_a(t). \tag{3.26}$$

In all models the exterior surface is traction free unless a displacement boundary is applied, as is at the clamps where the displacement is fixed. All models utilize the no-flux condition for all species transport equations and the superficial electrode model in (3.24). Under the electromechanical (actuator) model we have applied potential boundary conditions at the clamps, where the upper clamp is held at an applied potential that varies in time while the lower is held at zero for the ground potential. For mechanoelectrical (sensor) models we have a prescribed displacement along the forward face of the IPMC which serves as the driving input. For open-circuit voltage sensing we fix one electrode clamp at zero for a ground potential while the other is allowed to take on a floating potential. The floating potential clamp has zero current, which may be enforced via equation (3.25). Alternatively, the short-circuit sensor model exhibits both clamps' electric potential being equal (i.e. short-circuited) and we set this value to zero for simplicity.

In the open-circuit voltage sensing model we take the lower contact point between the clamp and electrode to be the ground voltage, and thus our sensing voltage response is obtained below. The order of the potential difference produces a positive open-circuit voltage when the IPMC is bent towards the upper electrode clamp.

$$\phi_{oc} = \phi_- - \phi_+ \rightarrow \phi_{oc} = -\phi_+. \tag{3.27}$$

For the short-circuit current sensor model, the total sensing current is the difference between the current passing into the lower $(-)$ and upper $(+)$ electrode clamps. This ordering produces a net short-circuit current outwards of the lower electrode in response to the IPMC bending towards the upper electrode clamp.

$$I_{sc} = I_- - I_+. \tag{3.28}$$

Using our superficial electrode model, the total current passing into either of the respective electrode clamps is found as the integral along the contact line, denoted $\Gamma_\pm$, between the clamp and electrode.

$$I_\pm = \int_{\Gamma_\pm} \underline{i}^S \cdot \underline{n}_C \mathrm{d}\ell \rightarrow \left(\underline{i}^S \cdot \underline{n}_C\right)_\pm w = -\left(\underline{\underline{\sigma}}_e^S \nabla_S\phi \cdot \underline{n}_C\right)_\pm w \tag{3.29}$$

where to the right of the arrow we have assumed a rectangular IPMC of width w and whose fields vary negligibly along the width direction. Further, the right most expression has shifted the dependence from surface current density onto the surface gradient of the electric potential, which is a field that will ultimately be calculated within the model.

We can formulate an alternative expression for the total current flowing through either contact by leveraging the interfacial charge conservation to transfer the contour integral in (3.29) into a surface integral along the entire polymer-electrode interface. This results in the total current flowing through each contact as

$$I_\pm = -w \int_{L_\pm} \frac{\partial}{\partial t}(\in \nabla\phi\cdot\underline{n})\,\mathrm{d}\ell \tag{3.30}$$

wherein $L_\pm$ is the length of the free IPMC on the upper $(+)$ and lower $(-)$ polymer-electrode interface, respectively. Hence, our total short-circuit sensing current may be calculated using either expression below.

Table 1. Material properties for IPMC COMSOL model.

Parameter	Value	Physical units	Description
l	40	[mm]	IPMC free length
w	10	[mm]	IPMC width
h	250	[μm]	IPMC thickness
ΔV	40	[%]	Volume uptake
EW	1100	$[\mathrm{g\ mol^{-1}}]$	Equivalent weight
$\in$	6	[mF]	Dielectric constant
$\mathcal{C}_E$	600	[MPa]	Young's modulus
$\mathcal{C}_\nu$	0.45	[−]	Poisson ratio
ρ_s	2000	$[\mathrm{kg\ m^{-3}}]$	Membrane density
$\mathcal{D}_+$	$1 \cdot 10^{-11}$	$[\mathrm{m^2\ s^{-1}}]$	Ionic self-diffusivity
$\mathcal{D}_w$	$7 \cdot 10^{-10}$	$[\mathrm{m^2\ s^{-1}}]$	Solvent self-diffusivity
z_+	1	[−]	Cation charge number
z_-	−1	[−]	Anion charge number
m_+	6.941	$[\mathrm{g\ mol^{-1}}]$	Cation molar mass
m_w	18.015	$[\mathrm{g\ mol^{-1}}]$	Solvent molar mass
v_+	1.297×10^{-5}	$[\mathrm{m^3\ mol^{-1}}]$	Cation molar volume
v_w	1.8×10^{-5}	$[\mathrm{m^3\ mol^{-1}}]$	Solvent molar volume
n_{dw}	4	[−]	Water transference/drag coefficient
ρ_w	1000	$[\mathrm{kg\ m^{-3}}]$	Water density
k_f	3×10^{-20}	$[\mathrm{m^2\ s^{-1}\ Pa}]$	Hydraulic permeability
r_e^S	0.03	[Ω]	Surface resistivity

$$I_{\mathrm{sc}} = -w\underline{\underline{\sigma}}_e^S\left((\nabla_S\phi\cdot\underline{n}_C)_- - (\nabla_S\phi\cdot\underline{n}_C)_+\right)$$
$$= -w\left(\int_{L_-}\frac{\partial}{\partial t}(\in\nabla\phi\cdot\underline{n})\,\mathrm{d}\ell - \int_{L_+}\frac{\partial}{\partial t}(\in\nabla\phi\cdot\underline{n})\,\mathrm{d}\ell\right). \tag{3.31}$$

3.5. Finite element modeling of IPMC electromechanical transduction

Preliminary simulation results using this new modeling framework are presented below. Here we consider the response of a cantilever IPMC to a 1 V step input to the upper electrode clamp. The model is implemented in COMSOL Multiphysics 5.6 on an Intel Core i5-4460S 2.90 GHz processor with 16 GB of RAM. The majority of the equations are formulated in an equation-based modeling approach, wherein the PDE interface built into COMSOL is used for the electrochemical equations, as well as the calculation of the conjugate pressure and porosity transport. The mechanical equations are solved in the COMSOL Solid Mechanics interface, with the stress coupling achieved using an External Stress interface. A complete set of physical properties used to describe the IPMC for this model are provided in table 1.

Shown in figure 4, the simulated IPMC exhibits the characteristic initial deformation towards the anode (positive in this instance, as the anode is the upper electrode), followed by a slower back-relaxation towards the cathode. The back-relaxation in this model is due to a combined effect of solvent back diffusion and the Maxwell stress, the latter of which being governed by the asymmetric cation concentration and

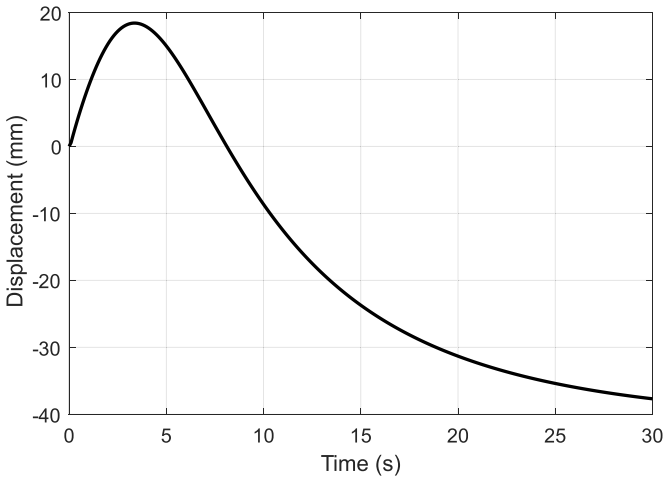

Figure 4. Time trace of IPMC transverse tip displacement in response to 1 V step input. The characteristic initial positive bending towards the anode of the IPMC followed by a slower back-relaxation is present in the simulated IPMC model.

electric potential at the electrode-polymer interfaces (See figures 5 and 6). The pronounced back-relaxation demonstrated above is found in similar multiphysics models that account for the Maxwell stress contribution to the overall Cauchy stress, and the bending past the initial state has been demonstrated in experimental studies of IPMC actuators [56, 95, 96, 100, 101]. A snapshot of the IPMC deformation is shown in figure 7 near the peak displacement response.

The free cation concentration evolves asymmetrically in the through-the-thickness direction at the cathode and anode due to the presence of anions fixed to the polymer backbone. Cation accumulation at the cathode is unbounded with increasing voltage due to the lack of steric effects [34, 102].

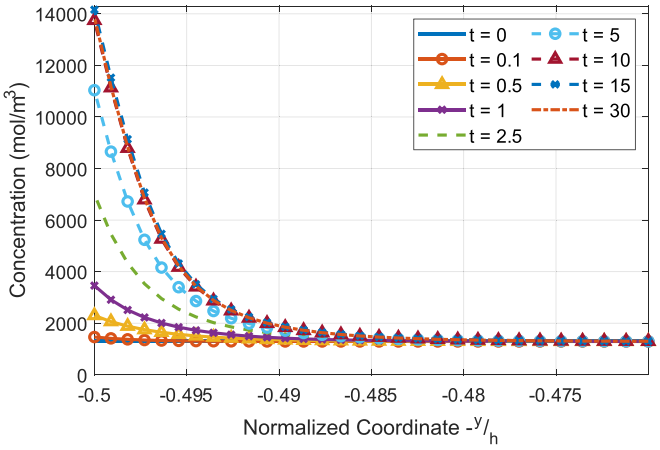

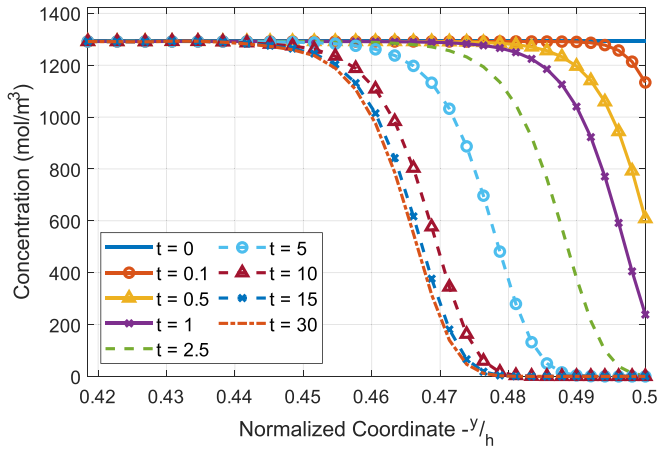

Figure 5. Evolution of concentration profile at anode and cathode of IPMC. The evolution of cation concentration at the clamped end of the IPMC for the cathode (above) and anode (below) are shown above. Results from COMSOL model are interpolated onto a uniform grid for plotting.

Upon close inspection, the cation concentration at the cathode shows the rapid increase towards a peak value, followed by a slight decrease due to the coupled transport and back diffusion of solvent water. Conversely, at the anode the cation depletion zone grows monotonically to its steady state. The electric potential across the thickness of the IPMC evolves in time with a linearly dominated profile in the bulk and the formation of boundary layers at both the cathode and anode electrode-polymer interfaces. The boundary layer formation are related to the governing equations being singularly perturbed in the spatial dimension [33, 103].

4. Dimensional analysis framework for IPMC transduction modeling

4.1. Dimensionless groups for IPMC actuators and sensors

We first develop groundwork for analyzing the electromechanical response for a cantilever IPMC through the lens of

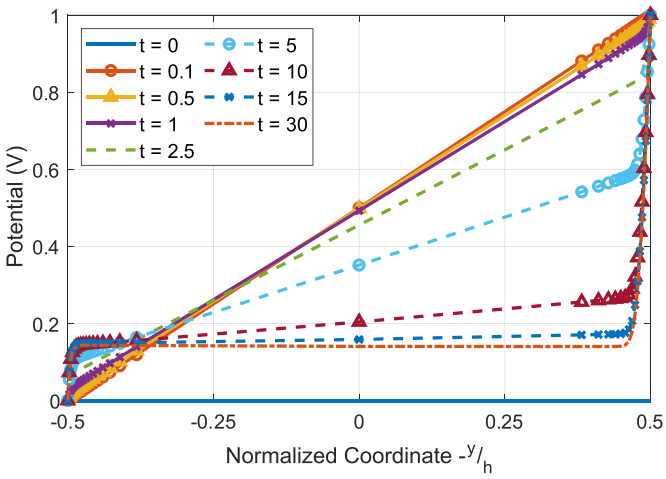

Figure 6. Evolution of electric potential profile at the IPMC clamp. The electric potential at the clamp rapidly grows at the anode to match the applied potential, and slowly stabilizes to the steady state profile as the external voltage is held. Results from COMSOL model are interpolated onto a non-uniform grid generated from a hyperbolic sine function for plotting.

dimensional analysis. We consider the transverse tip displacement, Δ, and blocking force, $\mathcal{R}$ (the reaction force constraining the IPMC strip). The transduction response will depend on the physical quantities we have established in our new modeling framework. The set of these physical quantities is partitioned into dimensionally independent, q_i, and dependent, q_d, subsets as described in tables 2 and 3, respectively, and we have chosen a fundamental unit system of mass (M), length (L), time (T), amount (N), current (I), and temperature (θ).

Using the principles of The Buckingham Π theorem and calculating of the null space of the Dimension matrix [104–107], we can formulate dimensionless Π-groups which allow us to reduce the number of independent parameters needed to quantify the behavior of the transverse tip deformation and blocking force. In this process, we obtain the following 17 dimensionless Π-groups.

$$\Pi_1 = \frac{c_{w,0}}{c_{+,0}},\ \Pi_2 = \frac{\mathcal{D}_w}{\mathcal{D}_+},\ \Pi_3 = \nu_+ c_{+,0},\ \Pi_4 = \frac{\nu_w}{\nu_+},$$

$$\Pi_5 = \frac{k_f \mathcal{C}_E}{\mathcal{D}_+},\ \Pi_6 = \frac{l}{h},\ \Pi_7 = \frac{\phi_{a,c}}{\phi_{th}},\ \Pi_8 = \frac{\in \left(\frac{\phi_{th}}{h}\right)^2}{\mathcal{C}_E},$$

$$\Pi_9 = \frac{RTc_{+,0}}{\mathcal{C}_E},\ \Pi_{10} = \mathcal{C}_\nu,\ \Pi_{11} = n_{dw},\ \Pi_{12} = \frac{\tau_\rho}{\tau_\mathcal{D}},$$

$$\Pi_{13} = \tau_\mathcal{D}\omega, \Pi_{14} = \frac{c_{-,0}}{c_{+,0}}, \Pi_{15} = z_+, \Pi_{16} = \frac{z_-}{z_+}, \Pi_{17} = \frac{\tau_{r_e}}{\tau_\mathcal{D}}. \tag{4.1}$$

In these definitions, we have formed a few key parameters that define these Π-groups. Namely, we have the thermal

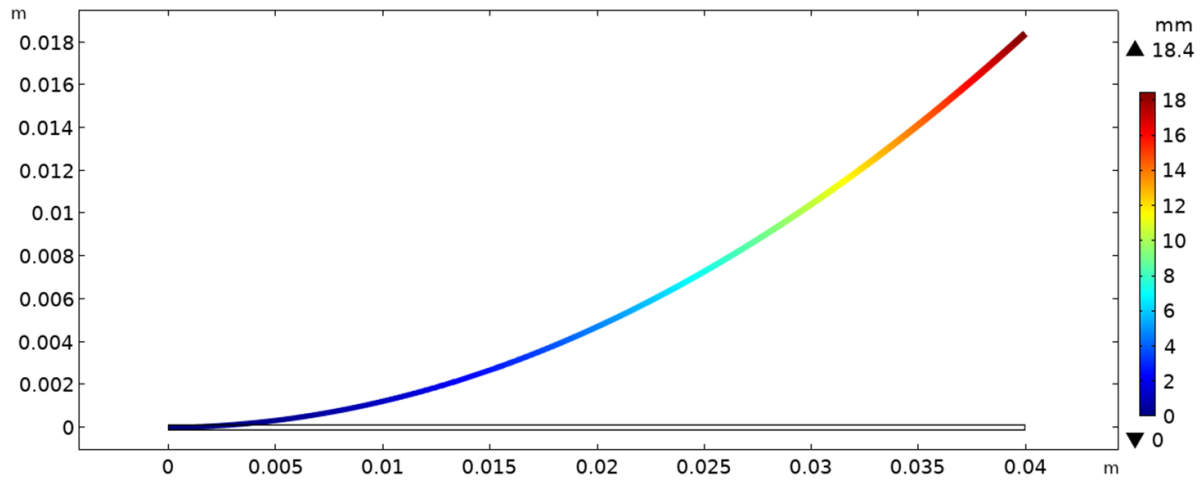

Figure 7. Snapshot of IPMC deformation response during 1 V step input. The deformed state of the IPMC at a time of $t = 3.4$ s is shown above, demonstrating the peak forward displacement obtained in response to the 1 V step input.

Table 2. Dimensionally independent subset of quantities for actuation.

Quantity	Fundamental units	Description
$c_{+,0}$	N/L^3	Initial cation concentration
h	L	IPMC thickness
$\phi_{a,c}$	ML^2/T^3I	Characteristic applied electric potential
$\in$	T^4I^2/ML^3	Dielectric constant
$\mathcal{D}_+$	L^2/T	Cation diffusivity
T	θ	Thermodynamic temperature

voltage $\phi_{\text{th}} = RT/\mathcal{F}$, and the characteristic timescales associated with diffusion, inertia, and resistivity, defined below.

$$\tau_{\mathcal{D}} = \frac{h^2}{\mathcal{D}_+}, \tau_\rho = \sqrt{\frac{\rho h l}{\mathcal{C}_E}}, \tau_{r_e} = \in hr_e^S. \tag{4.2}$$

Accounting for the initial electroneutrality of the IPMC we find an additional constraint which couples two of these Π-groups, emphasizing that they are not physically independent and hence the dimensionless transverse deformation is only a function of one of these parameters.

$$\Pi_{16} = -\frac{1}{\Pi_{14}} \tag{4.3}$$

This allows us to predict that the dimensionless transverse deformation (tip deflection scaled by the IPMC length), and dimensionless blocking force (scaled by an unspecified characteristic force) has the following functional dependence on our obtained Π-groups.

$$\Pi_\Delta = \frac{\Delta}{l} = f_\Delta\left(\Pi_{\{1-15,\,17\}}\right) \tag{4.4a}$$

$$\Pi_{\mathcal{R}} = \frac{\mathcal{R}}{F_c} = f_{\mathcal{R}}\left(\Pi_{\{1-15,\,17\}}\right). \tag{4.4b}$$

We may formulate a similar relation for mechanoelectrical response in terms of the short-circuit current and open-circuit voltage with nearly identical reasoning. The applied potential, which is the driving input for actuation, is replaced with a characteristic displacement which describes the deformation inducing the mechanoelectrical response. We partition the parameters into dimensionally independent and dependent subsets, provided in tables 4 and 5.

We obtain the same set of Π-groups as before, with the exception of Π_7 and Π_8, and find two new dimensionless groups.

$$\Pi_{18} = \frac{u_{a,c}}{l},\ \Pi_{19} = \frac{h}{\lambda_d}. \tag{4.5}$$

We can see Π_{18} as a direct replacement of Π_7 as the dimensionless input for this mode of transduction. In the denominator of Π_{19} we find the Debye screening length, defined below, and hence this dimensionless group expresses the ratio of IPMC thickness to the screening length.

$$\lambda_d = \frac{1}{\mathcal{F}}\sqrt{\frac{\in RT}{z_+^2 c_{+,0}}}. \tag{4.6}$$

The analysis for short-circuit current and open-circuit voltage are identical, the only difference being the exact nature the functional dependence would take in each case. Hence, we summarize the predicted dependence for short-circuit current and closed-circuit voltage as below.

$$\frac{I_{\text{sc}}}{I_{\text{sc},c}} = f_{\text{sc}}\left(\Pi_{\{1-6,\,9-15,\,17-19\}}\right) \tag{4.7a}$$

$$\frac{\phi_{\text{oc}}}{\phi_{\text{th}}} = f_{\text{oc}}\left(\Pi_{\{1-6,\,9-15,\,17-19\}}\right) \tag{4.7b}$$

where we have left the characteristic short-circuit current unspecified.

Table 3. Dimensionally dependent subset of quantities for actuation.

Quantity	Fundamental units	Description
$c_{w,0}$	N/L^3	Initial solvent concentration
$\mathcal{D}_w$	L^2/T	Solvent diffusivity
ν_+	L^3/N	Cation molar volume
ν_w	L^3/N	Solvent molar volume
k_f	L^3T/M	Membrane hydraulic permeability
l	L	IPMC length
$\mathcal{F}$	TI/N	Faraday's constant
$\mathcal{C}_E$	M/LT^2	IPMC elastic modulus
R	$ML^2/T^2N\theta$	Gas constant
$\mathcal{C}_\nu$	1	Membrane Poisson ratio
n_{dw}	1	Static water transference coefficient
ρ	M/L^3	IPMC mass density
ω	$1/T$	Driving frequency
$c_{-,0}$	N/L^3	Initial anion concentration
z_+	1	Cation charge number
z_-	1	Anion charge number
r_e^S	ML^2/T^3I^2	Electrode surface resistivity

Table 4. Dimensionally independent subset of quantities for sensing.

Quantity	Fundamental units	Description
$c_{+,0}$	N/L^3	Initial cation concentration
h	L	IPMC thickness
R	$ML^2/T^2N\theta$	Gas constant
$\in$	T^4I^2/ML^3	Dielectric constant
$\mathcal{D}_+$	L^2/T	Cation diffusivity
T	θ	Thermodynamic temperature

In table 6 we tabulate the Π-groups along with a short physical description and shorthand name which we will use to refer to each dimensionless number in future studies. These are intended to provide additional clarity when discussing these Π-groups by associating some of the physical underpinnings of their construction in the shorthand name. We highlight four specific dimensionless groups, namely the hydraulic number, Maxwell number, Omotic number, and resistive dynamics. These Π-groups are given the names Olsen-Kim 1, Olsen-Kim 2, Olsen-Kim 3, and Olsen-Kim 4 (OK# for short) as they represent fundamental physics in the transduction phenomena, their formulations have not been presented in IPMC literature, and later will be demonstrated as important characteristics for describing the transduction response.

On a final note, we pointed out that the driving voltage was replaced by the driving displacement as the input when we transition from electromechanical to mechanoelectrical transduction. We also found that the Maxwell Number was replaced with the reciprocal double layer. Here we demonstrate that these two dimensionless numbers cannot simultaneously exist in the set of physically independent Π-groups because they are in fact not physically independent from one another, which will come into play in the nondimensionalized governing equations which are developed in the next section.

Below we conduct a sequence of mathematical manipulations to the square of the reciprocal double layer, showing each step with enough detail to follow the process as this Π-group is transformed into a combination of those groups which arose in the actuator model, emphasizing the physical dependence of the Maxwell number and the reciprocal double layer.

$$\Pi_{19}^2 = \frac{h^2}{\lambda_d^2} = \frac{h^2}{\frac{1}{\mathcal{F}^2}\frac{\in RT}{z_+^2 c_{+,0}}} = h^2\mathcal{F}^2\frac{z_+^2 c_{+,0}}{\in RT} = z_+^2\frac{RTc_{+,0}}{\mathcal{C}_E}\frac{h^2\mathcal{C}_E}{\in\left(\frac{RT}{h\mathcal{F}}\right)^2}$$

$$= (z_+)^2\frac{RTc_{+,0}}{\mathcal{C}_E}\frac{\mathcal{C}_E}{\in\left(\frac{\phi_{\text{th}}}{h}\right)^2} = \frac{\Pi_{15}^2\Pi_9}{\Pi_8}. \tag{4.8}$$

4.2. Nondimensionalized field equations

Finally, we present the linearized governing differential equations in a nondimensional formulation and define characteristic fields to render these equations in terms of our newly obtained Π-groups. Each of the physical fields, along with the spatial coordinates and time, are nondimensionalized with respect to unspecified characteristic values (subscript c), and the dimensionless fields that define the equations are written with an accent hat.

$$x_i = x_c\hat{x}_i, \nabla = \frac{1}{x_c}\hat{\nabla}, \quad f = f_c\hat{f}. \tag{4.9}$$

We start with the electrical equations for the membrane and the polymer-electrode interface, which consist of Poisson's equation of electrostatics, the definition of electric displacement, and the superficial electrode model.

$$-\hat{\nabla}\cdot\hat{\nabla}\hat{\phi} = \frac{x_c^2\mathcal{F}}{\in\phi_c}z_+c_{+,c}\left(\hat{c}_+ + \frac{z_-}{z_+}\frac{c_{-,c}}{c_{+,c}}\hat{c}_-\right) \tag{4.10a}$$

$$d_c\underline{\hat{d}} = -\frac{\in\phi_c}{x_c}\hat{\nabla}\hat{\phi} \tag{4.10b}$$

Table 5. Dimensionally dependent subset of quantities for sensing.

Quantity	Fundamental units	Description
$c_{w,0}$	N/L^3	Initial solvent concentration
$\mathcal{D}_w$	L^2/T	Solvent diffusivity
ν_+	L^3/N	Cation molar volume
ν_w	L^3/N	Solvent molar volume
k_f	L^3T/M	Membrane hydraulic permeability
l	L	IPMC length
$\mathcal{F}$	TI/N	Faraday's constant
$\mathcal{C}_E$	M/LT^2	IPMC elastic modulus
$u_{a,c}$	L	Characteristic applied displacement
$\mathcal{C}_\nu$	1	Membrane Poisson ratio
n_{dw}	1	Static water transference coefficient
ρ	M/L^3	IPMC mass density
ω	$1/T$	Driving frequency
$c_{-,0}$	N/L^3	Initial anion concentration
z_+	1	Cation charge number
z_-	1	Anion charge number
r_e^S	ML^2/T^3I^2	Electrode surface resistivity

Table 6. List of dimensionless groups, physical descriptions, and shorthand names.

Dimensionless group	Physical description	Shorthand name
$\Pi_1 = \frac{c_{w,0}}{c_{+,0}}$	Initial ratio of solvent to mobile ionic species	Concentration number
$\Pi_2 = \frac{\mathcal{D}_w}{\mathcal{D}_+}$	Ratio of diffusivity in solvent and mobile ionic species	Diffusion number
$\Pi_3 = \nu_+ c_{+,0}$	Initial volume fraction of ionic species	Ionic fraction
$\Pi_4 = \frac{\nu_w}{\nu_+}$	Relative volume of solvent to ionic species on molar basis	Solvent size
$\Pi_5 = \frac{k_f \mathcal{C}_E}{\mathcal{D}_+}$	Hydraulic advection versus diffusive transport	Hydraulic number (Olsen-Kim 1)
$\Pi_6 = \frac{l}{h}$	Aspect ratio of IPMC as length vs thickness	Aspect ratio
$\Pi_7 = \frac{\phi_{a,c}}{\phi_{\text{th}}} = \frac{\mathcal{F}\phi_{a,c}}{RT}$	Driving input for IPMC actuator/electromigration	Driving potential
$\Pi_8 = \frac{\in \left(\frac{\phi_{\text{th}}}{h}\right)^2}{\mathcal{C}_E}$	Stress contribution due to electrostatic/Maxwell tensor	Maxwell number (Olsen-Kim 2)
$\Pi_9 = \frac{RTc_{+,0}}{\mathcal{C}_E}$	Stress contribution due to osmotic pressure	Osmotic number (Olsen-Kim 3)
$\Pi_{10} = \mathcal{C}_\nu$	Poisson ratio of linear elastic material	Poisson ratio
$\Pi_{11} = n_{dw}$	Number of solvent molecules transported via mobile ions	Solvent drag coefficient
$\Pi_{12} = \frac{\tau_\rho}{\tau_\mathcal{D}} = \frac{\mathcal{D}_+}{h^2}\sqrt{\frac{\rho h l}{\mathcal{C}_E}}$	Mechanical versus diffusive timescales	Mechanical dynamics
$\Pi_{13} = \tau_\mathcal{D}\omega = \frac{h^2\omega}{\mathcal{D}_+}$	Driving frequency for dynamic loading	Driving frequency
$\Pi_{14} = \frac{c_{-,0}}{c_{+,0}}$	Ratio of fixed to mobile ion concentration at electroneutrality	Electroneutrality number
$\Pi_{15} = z_+$	Charge number for mobile ionic species	Mobile charge number
$\Pi_{16} = \frac{z_-}{z_+}$	Ratio of charge numbers for fixed and mobile ionic species	Charge ratio
$\Pi_{17} = \frac{\tau_{r_e}}{\tau_\mathcal{D}} = \frac{\in r_e^S \mathcal{D}_+}{h}$	Resistive versus diffusive timescales	Resistive dynamics (Olsen-Kim 4)
$\Pi_{18} = \frac{u_{a,c}}{l}$	Driving input for IPMC sensor/advective migration	Driving displacement
$\Pi_{19} = \frac{h}{\lambda_d} = h\mathcal{F}\sqrt{\frac{z_+^2 c_{+,0}}{\in RT}}$	Ratio of ionomer thickness to Debye screening length	Reciprocal double layer

$$\hat{\nabla}_S \cdot \hat{\nabla}_S \hat{\phi} = \frac{\in x_c}{t_c} r_e^S \frac{\partial}{\partial \hat{t}} \left(\hat{\nabla}\hat{\phi} \cdot \underline{n} \right). \tag{4.10c}$$

Similarly, we have the mass conservation equations for the cation and solvent species along with the bulk fluid/porosity evolution.

$$\frac{x_c^2}{t_c \mathcal{D}_+} \frac{d\hat{c}_+}{d\hat{t}} = \hat{\nabla} \cdot \left(\hat{\nabla}\hat{c}_+ + \frac{\phi_c \mathcal{F}}{RT} z_+ \hat{c}_+ \hat{\nabla}\hat{\phi} + \frac{\nu_+ P_c}{RT} \hat{c}_+ \hat{\nabla}\widehat{P} + \frac{\mathcal{D}_w}{\mathcal{D}_+} \frac{c_{w,c}}{c_{+,c}} \hat{n}'_{d+} \left(\hat{\nabla}\hat{c}_w + \frac{\nu_w P_c}{RT} \hat{c}_w \hat{\nabla}\widehat{P} \right) + \frac{k_f p_c}{\mathcal{D}_+} \hat{c}_+ \hat{\nabla}\hat{p} \right) \tag{4.11a}$$

$$\frac{x_c^2}{t_c\mathcal{D}_+}\frac{c_{w,c}}{c_{+,c}}\frac{d\hat{c}_w}{\mathrm{d}\hat{t}} = \hat{\nabla}\cdot\left(\hat{n\prime}_{dw}\left(\hat{\nabla}\hat{c}_+ + \frac{\phi_c\mathcal{F}}{RT}z_+\hat{c}_+\hat{\nabla}\hat{\phi} + \frac{\nu_+P_c}{RT}\hat{c}_+\hat{\nabla}\widehat{P}\right) + \frac{\mathcal{D}_w}{\mathcal{D}_+}\frac{c_{w,c}}{c_{+,c}} \times\left(\hat{\nabla}\hat{c}_w + \frac{\nu_wP_c}{RT}\hat{c}_w\hat{\nabla}\widehat{P}\right) + \frac{c_{w,c}}{c_{+,c}}\frac{k_fp_c}{\mathcal{D}_+}\hat{c}_w\hat{\nabla}\hat{p}\right) \tag{4.11b}$$

$$\frac{x_c^2}{t_ck_fp_c}\frac{d}{\mathrm{d}\hat{t}}\left(\hat{\rho}_f^*\lambda\right) = \hat{\nabla}\cdot\left(\hat{\rho}_f^*\left(\frac{RTc_{+,c}}{p_c}\left(\hat{\nabla}\hat{c}_+ + \frac{\phi_c\mathcal{F}}{RT}z_+\hat{c}_+\hat{\nabla}\hat{\phi} + \frac{c_{w,c}}{c_{+,c}}\hat{\nabla}\hat{c}_w\right) + \hat{\lambda}\hat{\nabla}\left(\hat{p}+\frac{P_c}{p_c}\widehat{P}\right)\right)\right). \tag{4.11c}$$

We note that the dynamic ion and solvent transference coefficients, n'_{d+} and n'_{dw} are functions of the constituent species and their diffusivities. While these coefficients are already dimensionless, under the characteristic scaling we have a 'nondimensionalized' form of each defined below.

$$\hat{n\prime}_{d+} = \begin{cases} \dfrac{\mathcal{D}_+c_{+,0}}{\mathcal{D}_wc_{w,0}}n_{dw} & \dfrac{c_{+,c}}{c_{w,c}}\dfrac{\hat{c}_+}{\hat{c}_w} > \frac{1}{\gamma} \\ \dfrac{\hat{c}_+}{\hat{c}_w}\dfrac{\mathcal{D}_+c_{+,c}}{\mathcal{D}_wc_{w,c}}n_{dw} & \dfrac{c_{+,c}}{c_{w,c}}\dfrac{\hat{c}_+}{\hat{c}_w} \le \frac{1}{\gamma} \end{cases},$$

$$n\prime_{dw} = \begin{cases} \dfrac{\hat{c}_w}{\hat{c}_+}\dfrac{\mathcal{D}_wc_{w,c}}{\mathcal{D}_+c_{+,c}}n_{d+} & \dfrac{c_{+,c}}{c_{w,c}}\dfrac{\hat{c}_+}{\hat{c}_w} > \dfrac{1}{\gamma} \\ n_{dw} & \dfrac{c_{+,c}}{c_{w,c}}\dfrac{\hat{c}_+}{\hat{c}_w} \le \frac{1}{\gamma} \end{cases}. \tag{4.12}$$

Next, we nondimensionalize the mechanical equations for the IPMC. Starting with the equilibrium equation, and then moving onto the Cauchy stress tensor and its additive components.

$$\left(1-\hat{\lambda}_0\right)\frac{\rho_{s,0}^*x_cu_c}{\sigma_ct_c^2}\frac{\mathrm{d}^2\hat{\underline{u}}}{\mathrm{d}\hat{t}^2} = \hat{\nabla}\cdot\hat{\underline{\underline{\sigma}}}^T. \tag{4.13}$$

The total stress is additively composed of mechanical, ionic, polarization, and volumetric contributions, and hence the nondimensional stress tensor is written as

$$\hat{\underline{\underline{\sigma}}} = \hat{\underline{\underline{\sigma}}}_{\mathrm{mech}} + \hat{\underline{\underline{\sigma}}}_{\mathrm{ion}} + \hat{\underline{\underline{\sigma}}}_{\mathrm{pol}} + \hat{\underline{\underline{\sigma}}}_{\mathrm{vol}}. \tag{4.14}$$

Each of these components may scaled by the characteristic stress, with the other fields being scaled by their respective characteristic values.

$$\begin{aligned}
\hat{\underline{\underline{\sigma}}}_{\mathrm{mech}} &= \frac{2\mu_L}{\sigma_c}\left(\frac{\lambda_L}{2\mu_L}tr\left(\hat{\underline{\underline{\varepsilon}}}\right)\underline{\underline{I}} + \hat{\underline{\underline{\varepsilon}}}\right), \\
\hat{\underline{\underline{\sigma}}}_{\mathrm{pol}} &= \frac{d_c^2}{\varepsilon\sigma_c}\left(\hat{\underline{d}}\otimes\hat{\underline{d}} - \frac{1}{2}\left(\hat{\underline{d}}\cdot\hat{\underline{d}}\right)\underline{\underline{I}}\right) \\
\hat{\underline{\underline{\sigma}}}_{\mathrm{ion}} &= \frac{RTc_{+,c}}{\sigma_c}\left(\left(\frac{c_{+,0}}{c_{+,c}} - \hat{c}_+\right) + \frac{c_{w,c}}{c_{+,c}}\left(\frac{c_{w,0}}{c_{w,c}} - \hat{c}_w\right)\right)\underline{\underline{I}}, \\
\hat{\underline{\underline{\sigma}}}_{\mathrm{vol}} &= -\frac{\mathscr{P}_c}{\sigma_c}\hat{\mathcal{P}}\underline{\underline{I}}.
\end{aligned} \tag{4.15}$$

The strain tensor is already nondimensional, but we still enforce the scaling of the displacement and length scale to write the 'nondimensional' form below.

$$\hat{\underline{\underline{\varepsilon}}} = \frac{1}{2}\frac{u_c}{x_c}\left(\hat{\nabla}\hat{\underline{u}} + \left(\hat{\nabla}\hat{\underline{u}}\right)^T\right). \tag{4.16}$$

We also note that the volume contribution is written in terms of the characteristic conjugate pressure, which is itself nondimensionalized below. The bulk modulus $\mathcal{C}_K$ is written in terms of the Young's modulus and Poisson ratio, $\mathcal{C}_E$ and $\mathcal{C}_\nu$, respectively.

$$\hat{\mathscr{P}} = -\frac{1}{3}\frac{\mathcal{C}_E}{\mathscr{P}_c}\frac{1}{(1-2\mathcal{C}_\nu)}\frac{1}{1-\hat{\lambda}}\left(\frac{\hat{\lambda}_0-\hat{\lambda}}{1-\hat{\lambda}_0} + \frac{u_c}{x_c}\hat{\nabla}\cdot\hat{\underline{u}}\right). \tag{4.17}$$

The nondimensional relation between conjugate, hydrostatic, and Lagrange pressure also has a unique form under the characteristic scaling, where we allow for distinct characteristic values for each of the pressure terms for the sake of generality.

$$\hat{\mathscr{P}} = \frac{p_c}{\mathscr{P}_c}\left(\hat{p} + \frac{\mathcal{P}_c}{\mathscr{P}_c}\widehat{P}\right). \tag{4.18}$$

Lastly, we look at the porosity as represented in terms of the characteristic scaling.

$$\begin{aligned}
\hat{\lambda}_0 &= \nu_+c_{+,c}\left(\frac{c_{+,0}}{c_{+,c}} + \frac{\nu_w}{\nu_+}\frac{c_{w,c}}{c_{+,c}}\frac{c_{w,0}}{c_{w,c}}\right), \\
\hat{\lambda} &= \nu_+c_{+,c}\left(\hat{c}_+ + \frac{\nu_w}{\nu_+}\frac{c_{w,c}}{c_{+,c}}\hat{c}_w\right).
\end{aligned} \tag{4.19}$$

4.3. Characteristic field measures

We now identify the characteristic values for the fields that govern the nondimensional equations. Starting with the characteristic length scale for derivatives, it is well known that IPMC materials exhibit strong gradients along the thickness direction, but near negligible gradients in the other orthogonal directions. Hence, we consider the IPMC thickness as the

length scale for spatial derivatives that arise within the membrane ($x_c := h$) while the IPMC length is used to nondimensionalize the displacement field ($u_c := l$). The molar concentrations are reasonably normalized according to their initial values ($c_{\beta,c} := c_{\beta,0}$).

From the nondimensional mechanical contribution to the stress, we propose that the stress be normalized with respect to the Young's modulus of the material. Similarly, from the contribution from the conjugate pressure, we propose that a characteristic value based on the characteristic stress. Further, from the nondimensional relation for the various pressure terms, we propose that all of the pressures share a single characteristic value (i.e. $p_c = \not{p}_c = P_c = \sigma_c := \mathcal{C}_E$).

The polarization contribution introduced a characteristic electric displacement. This may be defined in terms of a characteristic electric field, and hence potential, across the ionomer thickness. Making the choice of assigning the characteristic potential as the thermal voltage, we have a characteristic electric displacement defined below.

$$d_c := -\in \frac{\phi_{\text{th}}}{h}. \tag{4.20}$$

With these choices, we find four distinct characteristic timescales, namely:

$$t_{c,1} = \tau_{\mathcal{D}}, \quad t_{c,2} = \tau_{\rho}, t_{c,3} = \frac{h^2}{k_f \mathcal{C}_E} = \tau_{k_f}, \quad t_{c,4} = \tau_{r_e}. \tag{4.21}$$

The third is a new timescale associated with the inertial effects of the fluid phase, which is related to the diffusion time constant through the Hydraulic Number. As is often the case when working with nondimensional equations, a given choice of scales may result in equations that are more or less difficult to analyze when compared to another choice scale. There is yet another possible timescale that is important to mention which may be derived from the diffusion timescale. Leveraging the relation between the IPMC thickness and Debye screening length, we define an additional timescale which is commonly used within the literature.

$$t_{c,5} = \frac{t_{c,1}}{\Pi_{19}} = \frac{h\lambda_d}{\mathcal{D}_+} = \tau_{\lambda_d}. \tag{4.22}$$

In fact, this is the same scale used in [103] that aided the use of matched asymptotic expansion, which ultimately resulted in a semi-analytical solutions to the IPMC electrochemistry.

4.4. Dimensionless groups in the governing multiphysics equations

We opt to use the diffusional timescale ($t_c := \tau_d$) for our characteristic measure. With this choice, along with the chosen characteristic field measures just described, we obtain the following set of dimensionless governing equations which are written in terms of our formulated Π-groups.

$$-\hat{\nabla}\cdot\hat{\nabla}\hat{\phi} = \frac{\Pi_{15}\Pi_9}{\Pi_8}\left(\hat{c}_+ - \hat{c}_-\right),\ \hat{c}_- = 1,\ \hat{\underline{d}} = \hat{\nabla}\hat{\phi} \tag{4.23a}$$

$$\hat{\nabla}_S\cdot\hat{\nabla}_S\hat{\phi} = \Pi_{17}\frac{\partial}{\partial\hat{t}}\left(\hat{\nabla}\hat{\phi}\cdot\underline{n}\right) \tag{4.23b}$$

$$\frac{d\hat{c}_+}{\mathrm{d}\hat{t}} = \hat{\nabla}\cdot\left(\hat{\nabla}\hat{c}_+ + \Pi_{15}\hat{c}_+\hat{\nabla}\hat{\phi} + \frac{\Pi_3}{\Pi_9}\hat{c}_+\hat{\nabla}\widehat{P} + \Pi_1\Pi_2\hat{n}'_{d+} \times\left(\hat{\nabla}\hat{c}_w + \frac{\Pi_3\Pi_4}{\Pi_9}\hat{c}_w\hat{\nabla}\widehat{P}\right) + \Pi_5\hat{c}_+\hat{\nabla}\hat{p}\right) \tag{4.23c}$$

$$\frac{d\hat{c}_w}{\mathrm{d}\hat{t}} = \hat{\nabla}\cdot\left(\frac{\hat{n}'_{dw}}{\Pi_1}\left(\hat{\nabla}\hat{c}_+ + \Pi_{15}\hat{c}_+\hat{\nabla}\hat{\phi} + \frac{\Pi_3}{\Pi_9}\hat{c}_+\hat{\nabla}\widehat{P}\right) + \Pi_2 \times\left(\hat{\nabla}\hat{c}_w + \frac{\Pi_3\Pi_4}{\Pi_9}\hat{c}_w\hat{\nabla}\widehat{P}\right) + \Pi_5\hat{c}_w\hat{\nabla}\hat{p}\right) \tag{4.23d}$$

$$\frac{d\hat{\lambda}}{\mathrm{d}\hat{t}} = \Pi_5\hat{\nabla}\cdot\left(\Pi_9\left(\hat{\nabla}\hat{c}_+ + \Pi_{15}\hat{c}_+\hat{\nabla}\hat{\phi} + \Pi_1\hat{\nabla}\hat{c}_w\right) + \hat{\lambda}\hat{\nabla}\hat{p}\right) \tag{4.23e}$$

$$\hat{n}'_{d+} = \begin{cases} \dfrac{\Pi_{11}}{\Pi_1\Pi_2} & \dfrac{\hat{c}_+}{\hat{c}_w} > \dfrac{\Pi_1\Pi_2}{\Pi_{11}^2} \\ \dfrac{\Pi_{11}}{\Pi_1\Pi_2}\dfrac{\hat{c}_+}{\hat{c}_w} & \dfrac{\hat{c}_+}{\hat{c}_w} \le \dfrac{\Pi_1\Pi_2}{\Pi_{11}^2} \end{cases},$$

$$\hat{n}'_{dw} = \begin{cases} \Pi_{11}\dfrac{\hat{c}_w}{\hat{c}_+} & \dfrac{\hat{c}_+}{\hat{c}_w} > \dfrac{\Pi_1\Pi_2}{\Pi_{11}^2} \\ \Pi_{11} & \dfrac{\hat{c}_+}{\hat{c}_w} \le \dfrac{\Pi_1\Pi_2}{\Pi_{11}^2} \end{cases} \tag{4.23f}$$

$$\left(1-\hat{\lambda}_0\right)\Pi_{12}^2\frac{d^2\hat{\underline{u}}}{d\hat{t}^2} = \hat{\nabla}\cdot\hat{\underline{\underline{\sigma}}}^T \tag{4.23g}$$

$$\hat{\underline{\underline{\sigma}}}_{\text{mech}} = \frac{1}{1+\Pi_{10}}\left(\frac{\Pi_{10}}{1-2\Pi_{10}}tr\left(\hat{\underline{\underline{\varepsilon}}}\right)\underline{\underline{I}} + \hat{\underline{\underline{\varepsilon}}}\right),\ \hat{\underline{\underline{\sigma}}}_{\text{vol}} = -\hat{p}\underline{\underline{I}} \tag{4.23h}$$

$$\hat{\underline{\underline{\sigma}}}_{\text{ion}} = \Pi_9\left[\left(1-\hat{c}_+\right) + \Pi_1\left(1-\hat{c}_w\right)\right]\underline{\underline{I}},$$
$$\hat{\underline{\underline{\sigma}}}_{\text{pol}} = \Pi_8\left(\hat{\underline{d}}\otimes\hat{\underline{d}} - \frac{1}{2}\left(\hat{\underline{d}}\cdot\hat{\underline{d}}\right)\underline{\underline{I}}\right) \tag{4.23i}$$

$$\hat{p} = -\frac{1}{3}\frac{1}{\left(1-2\Pi_{10}\right)}\frac{1}{1-\hat{\lambda}}\left(\frac{\hat{\lambda}_0-\hat{\lambda}}{1-\hat{\lambda}_0} + \Pi_6\hat{\nabla}\cdot\hat{\underline{u}}\right),\ \hat{p} = \hat{p} - \widehat{P} \tag{4.23j}$$

$$\hat{\lambda}_0 = \Pi_3\left(1+\Pi_1\Pi_4\right),\ \hat{\lambda} = \Pi_3\left(\hat{c}_+ + \Pi_1\Pi_4\hat{c}_w\right) \tag{4.23k}$$

$$\hat{\underline{\underline{\varepsilon}}} = \frac{1}{2}\Pi_6\left(\hat{\nabla}\hat{\underline{u}} + \left(\hat{\nabla}\hat{\underline{u}}\right)^T\right). \tag{4.23l}$$

The mechanical contribution to the Cauchy stress tensor has also been written in terms of the Young's modulus and Poisson's ratio prior to nondimensionalization. The above equations are written in terms of the Π-groups obtained for electromechanical transduction. As demonstrated earlier, the mechanoelectrical transduction gave an alternative set of Π-groups which govern the phenomenon. We already showed that the Driving Potential is replaced by the driving displacement as the input, and that the reciprocal double layer is not physically independent from the Osmotic number, Maxwell number, and mobile charge number. We can use these relations to recast the above equations into the forms below that utilize only the Π-groups that were predicted in the initial dimensional analysis with the Buckingham Π theorem. Only those equations which exhibit a change in form are reiterated below.

$$-\hat{\nabla}\cdot\hat{\nabla}\hat{\phi} = \frac{\Pi_{19}^2}{\Pi_{15}}\left(\hat{c}_+ - \hat{c}_-\right), \quad \underline{\underline{\hat{\sigma}}}_{\text{pol}} = \Pi_9\left(\frac{\Pi_{15}}{\Pi_{19}}\right)^2\left(\underline{\hat{d}}\otimes\underline{\hat{d}} - \frac{1}{2}\left(\underline{\hat{d}}\cdot\underline{\hat{d}}\right)\underline{\underline{I}}\right). \tag{4.24}$$

On a final note, the relationship established in equation (4.3) eliminates both Π_{14} and Π_{16} from equations (4.23*a*) and (4.24) rendering the system of governing equations invariant to both Π-groups and hence the functional relationships predicted by the dimensional analysis will not depend on either dimensionless number.

The mechanical boundary conditions translate into this dimensionless framework easily, as we only use traction free or zero-displacement conditions in the actuator model. Our boundary condition for the applied voltage during actuation transforms as:

$$\phi_{\text{anode}} = \phi_a(t) \rightarrow \hat{\phi}_{\text{anode}} = \Pi_7\hat{\phi}_a\left(t_c\hat{t}\right) \tag{4.25}$$

wherein the general time dependent function $\hat{\phi}_a\left(t_c\hat{t}\right)$ is scaled to have a characteristic amplitude of unity and in time with respect to our characteristic timescale. We see that Π_7 operates to increase the applied potential in the boundary condition, as expected.

In the mechanoelectrical model we use a prescribed displacement condition along the tip of the IPMC and find Π_{18} as part of the driving input as would be expected.

$$u_{y,\text{tip}} = u_a(t) \rightarrow \hat{u}_{y,\text{tip}} = \Pi_{18}\hat{u}_a\left(t_c\hat{t}\right). \tag{4.26}$$

The nondimensionalization of the sensing metrics for both short-circuit current and open-circuit voltage are similarly formulated. Under our nondimensional framework, the dimensionless forms of the sensing current expressions are rendered below.

$$\hat{I}_{\text{sc}} = -\frac{1}{\Pi_{17}}\left(\left(\hat{\nabla}_S\hat{\phi}\cdot\underline{n}_C\right)_- - \left(\hat{\nabla}_S\hat{\phi}\cdot\underline{n}_C\right)_+\right) \tag{4.27a}$$

$$\hat{I}_{\text{sc}} = -\left(\int_{\hat{L}_-}\frac{\partial}{\partial\hat{t}}\left(\hat{\nabla}\hat{\phi}\cdot\underline{n}\right)\mathrm{d}\hat{\ell} - \int_{\hat{L}_+}\frac{\partial}{\partial\hat{t}}\left(\hat{\nabla}\hat{\phi}\cdot\underline{n}\right)\mathrm{d}\hat{\ell}\right) \tag{4.27b}$$

wherein we implicitly defined the characteristic measure for total current as

$$I_{\text{sc},c} = \frac{w\in\phi_c}{\tau_{\mathcal{D}}}. \tag{4.28}$$

In the limit of lossless electrodes (i.e. $\Pi_{17}\rightarrow 0$) the electric potential along the length of each electrode is expected to be constant, and the first expression results in an indeterminant limit of zero divide zero. Hence, the latter is more robust for computing the short-circuit current in that under an assumption of lossless electrodes the expression remains well behaved. The dimensionless sensing voltage is simpler and calculated as

$$\hat{\phi}_{\text{oc}} = -\hat{\phi}_+. \tag{4.29}$$

5. Conclusion

Thus far, IPMC modeling literature has presented only a handful of multiphysics models that account for the coupled solvent/ion transport. Some models have been proposed, and in fact rederived under this framework, for the coupled transport without the robustness of a hyperelastic and thermodynamic free energy based formulation [21, 43]. Frameworks for modeling the electrochemical behavior of IPMCs using porous media methods have also been formulated [54], but models for porous IPMCs undergoing deformation are limited [55]. As recent as this year, new efforts have given rise to the closest model to ours which leverages the saturation condition in the volumetric strain of the membrane in a compressible material model [56].

The model developed here differs in the enforcement of the saturation condition as volume contributions to the bulk pore fluid. This approach allows for different mixture theory models to be easily implemented, as relaxing the ideal mixture assumption would amount to including equations of state for the volumetric contributions from solvent and ionic species to the pore fluid. In this work the newly developed model encompasses nearly all multiphysics formulations currently found in literature, allowing for new hyperelastic material models to be applied and rich solvent/ion interactions to be modeled under a single framework.

Using an additively decompose Helmholtz free energy, the constitutive equations derived under the new framework gave rise to a complete multiphysics model for the IPMC actuator and sensor under with aspects from porous media and coupled solvent/ion transport. We have presented the most general nondimensionalization of the obtained governing equations, along with an extensive collection of dimensionless groups that describe the IPMC transduction. Using our characteristic field measures we formulate a complete set of kinematically linear governing equations in a nondimensional framework with our specified Π-groups, which have yet to be derived

in the current IPMC literature. The generality of the nondimensionalized equations prior to defining the characteristic fields allows for future works to explore alternative scaling's which may render the equations more tractable. Our formulation may be used to conduct an extensive characterization of the electromechanical and mechanoelectrical transduction behavior for IPMCs in future studies.

The governing equations presented in this work may be extended to analyze the frequency response of the IPMC under both electromechanical and mechanoelectrical transduction. As is done throughout literature, an integral transforms (Laplace and Fourier) in the complex domain specified to the imaginary axis provide a powerful tool for translating the governing PDEs into the frequency domain for analyzing the dynamic behavior of the IPMC [35, 46, 82, 108, 109]. The model as derived in this study encompasses the effects of resistive electrodes and coupled ion-solvent transport undergoing large deformations. The kinematically linearized equations are restricted to small strain deformations of the IPMC material, and as such have some limitations in their predictive capabilities for high performance IPMCs exhibiting large actuation strokes. Furthermore, the set of governing equations derived utilized a Saint Venant-Kirchhoff material, limiting the models capability to fully predict effects found in other hyperelastic material models [56]. This may have an effect on the precited dynamics of the IPMC, and its frequency response to dynamic inputs.

As demonstrated in the finite element implementation, the model relies on many physical parameters making validation of the model an important and challenging question. This is one area where the nondimensional equations provide powerful tools for researchers. The use of dimensional analysis techniques may be used to reduce the number of free parameters in the model and hence required for validations. Furthermore, results obtained under a nondimensional setting are applicable to a wider range of physical IPMCs using the Π-groups in conjunction with material property characterization to translate the results form a nondimensional to dimensional setting. The current set of multiphysics equations may be used to conduct a broad characterization of the IPMC transduction response in a nondimensional setting, the results of such a study may then be validated against experiments on physical IPMCs in a similar nondimensional setting.

Data availability statement

The data that support the findings of this study are available upon reasonable request from the authors.

Acknowledgments

The authors acknowledge the partial financial support from the US National Science Foundation (NSF), Partnerships for International Research and Education (PIRE) Program, Grant No. 1545857. Any opinions, findings and conclusions or recommendations expressed in this material are those of the author(s) and do not necessarily reflect the views of the NSF.

ORCID iDs

Zakai J Olsen https://orcid.org/0000-0002-4499-6677
Kwang J Kim https://orcid.org/0000-0003-2134-4964

References

[1] Bar-Cohen Y 2002 Electroactive polymers as artificial muscles: a review *J. Spacecr. Rockets* **39** 822–7
[2] Hines L, Petersen K, Lum G Z and Sitti M 2017 Soft actuators for small-scale robotics *Adv. Mater.* **29**
[3] Shahinpoor M, Bar-Cohen Y, Simpson J O and Smith J 1998 Ionic polymer-metal composites (IPMCs) as biomimetic sensors, actuators-artificial muscles - a review *Smart Mater. Struct.* **7** R15–R30
[4] Kim K J, Yim W, Paquette J W and Kim D 2007 Ionic polymer-metal composites for underwater operation *J. Intell. Mater. Syst. Struct.* **18** 123–31
[5] Shahinpoor M 1992 Conceptual design, kinematics and dynamics of swimming robotic structures using ionic polymeric gel muscles *Smart Mater. Struct.* **1** 91–4
[6] Yim W, Lee J and Kim K J 2007 An artificial muscle actuator for biomimetic underwater propulsors *Bioinspir. Biomim.* **2** S31–S41
[7] Shahinpoor M and Kim K J 2001 Ionic polymer-metal composites: I. Fundamentals *Smart Mater. Struct.* **10** 819–33
[8] Kim K J and Shahinpoor M 2003 Ionic polymer-metal composites: II. Manufacturing techniques *Smart Mater. Struct.* **12** 65–79
[9] Shahinpoor M and Kim K J 2004 Ionic polymer-metal composites: III. Modeling and simulation as biomimetic sensors, actuators, transducers, and artificial muscles *Smart Mater. Struct.* **13** 1362–88
[10] Shahinpoor M and Kim K J 2005 Ionic polymer-metal composites: IV. Industrial and medical applications *Smart Mater. Struct.* **14** 197–214
[11] Jo C, Pugal D, Oh I-K, Kim K J and Asaka K 2013 Recent advances in ionic polymer-metal composite actuators and their modeling and applications *Prog. Polym. Sci.* **38** 1037–66
[12] Tiwari R and Garcia E 2011 The state of understanding of ionic polymer metal composite architecture: a review *Smart Mater. Struct.* **20** 083001
[13] Kim K J 2007 Ionic polymer-metal composite as a new actuator and transducer material *Electroactive Polymers for Robotic Applications* ed K J Kim and S Tadokoro (London: Springer) pp 153–64
[14] Bahramzadeh Y and Shahinpoor M 2014 A review of ionic polymeric soft actuators and sensors *Soft Robot.* **1** 38–52
[15] Eisenberg A 1970 Clustering of ions in organic polymers. A theoretical approach *Macromolecules* **3** 147–54
[16] Li J Y and Nemat-Nasser S 2000 Micromechanical analysis of ionic clustering in nafion perfluorinated membrane *Mech. Mater.* **32** 303–14
[17] Hsu W Y and Gierke T D 1982 Elastic theory for ionic clustering in perfluorinated ionomers *Macromolecules* **15** 101–5
[18] Datye V K, Taylor P L and Hopfinger A J 1984 Simple model for clustering and ionic transport in ionomer membranes *Macromolecules* **17** 1704–8
[19] Trabia S, Olsen Z and Kim K J 2017 Searching for a new ionomer for 3D printable ionic polymer–metal composites: aquivion as a candidate *Smart Mater. Struct.* **26** 115029
[20] Trabia S, Choi K, Olsen Z, Hwang T, Nam J-D and Kim K J 2018 Understanding the thermal properties of precursor-ionomers to optimize fabrication processes for ionic polymer-metal composites (IPMCs) *Materials* **11** 665

[21] Zhu Z, Chen H, Chang L and Li B 2011 Dynamic model of ion and water transport in ionic polymer-metal composites *AIP Adv.* **1** 040702

[22] Roth R and Gillespie D 2005 Physics of size selectivity *Phys. Rev. Lett.* **95** 9–12

[23] Minton G 2013 *Modelling the Static and Dynamic Behaviour of Electrolytes : A Modified Poisson-Nernst-Planck Approach* (Manchester: University of Manchester)

[24] Samoilov O 1953 Hydration of ions in aqueous solution *Bull. Acad. Sci. USSR, Div. Chem. Sci.* **2** 219–25

[25] Nemat-Nasser S and Wu Y 2003 Comparative experimental study of ionic polymer-metal composites with different backbone ionomers and in various cation forms *J. Appl. Phys.* **93** 5255–67

[26] Eigen M and Wicke E 1954 The thermodynamics of electrolytes at higher concentration *J. Phys. Chem.* **58** 702–14

[27] Burak Y and Andelman D 2000 Hydration interactions: aqueous solvent effects in electric double layers *Phys. Rev.* E **62** 5296–312

[28] Spiegler K S 1958 Transport processes in ionic membranes *Trans. Faraday Soc.* **54** 1408–28

[29] Bonomo C, Fortuna L, Giannone P, Graziani S and Strazzeri S 2007 A nonlinear model for ionic polymer metal composites as actuators *Smart Mater. Struct.* **16** 1–12

[30] Shahinpoor M, Bar-Cohen Y, Simpson J O and Smith J 1998 Ionic polymer-metal composites (IPMCs) as biomimetic sensors, actuators and artificial muscles—a review *Smart Mater. Struct.* **7** R15–R30

[31] Madden J D W, Vandesteeg N A, Anquetil P A, Madden P G A, Takshi A, Pytel R Z, Lafontaine S R, Wieringa P A and Hunter I W 2004 Artificial muscle technology: physical principles and naval prospects *IEEE J. Ocean. Eng.* **29** 706–28

[32] Nemat-Nasser S and Li J Y 2000 Electromechanical response of ionic polymer-metal composites *J. Appl. Phys.* **87** 3321–31

[33] Cha Y and Porfiri M 2014 Mechanics and electrochemistry of ionic polymer metal composites *J. Mech. Phys. Solids* **71** 156–78

[34] Porfiri M, Sharghi H and Zhang P 2018 Modeling back-relaxation in ionic polymer metal composites: the role of steric effects and composite layers *J. Appl. Phys.* **123** 014901

[35] Bahramzadeh Y and Shahinpoor M 2011 Dynamic curvature sensing employing ionic-polymer-metal composite sensors *Smart Mater. Struct.* **20** 094011

[36] Lim C, Lei H and Tan X 2012 A dynamic physics-based model for base-excited IPMC sensors *Electroactive Polymer Actuators and Devices (EAPAD) 2012* ed Y Bar-Cohen (https://doi.org/10.1117/12.915753)

[37] Branco P J C and Dente J A 2006 Derivation of a continuum model and its electric equivalent-circuit representation for ionic polymer-metal composite (IPMC) electromechanics *Smart Mater. Struct.* **15** 378–92

[38] Bonomo C, Fortuna L, Giannone P, Graziani S and Strazzeri S 2006 A model for ionic polymer metal composites as sensors *Smart Mater. Struct.* **15** 749–58

[39] Porfiri M 2009 An electromechanical model for sensing and actuation of ionic polymer metal composites *Smart Mater. Struct.* **18** 015016

[40] Aureli M and Porfiri M 2013 Nonlinear sensing of ionic polymer metal composites *Contin. Mech. Thermodyn.* **25** 273–310

[41] De Gennes P G, Okumura K, Shahinpoor M and Kim K J 2000 Mechanoelectric effects in ionic gels *Europhys. Lett.* **50** 513–8

[42] Schicker D and Wallmersperger T 2013 Modeling and simulation of the chemo-electro-mechanical behavior of ionic polymer-metal composites *J. Appl. Phys.* **114** 163709

[43] Zhu Z, Asaka K, Chang L, Takagi K and Chen H 2013 Multiphysics of ionic polymer-metal composite actuator *J. Appl. Phys.* **114**

[44] Paquette J W, Kim K J, Nam J-D and Tak Y S 2003 An equivalent circuit model for ionic polymer-metal composites and their performance improvement by a clay-based polymer nano-composite technique *J. Intell. Mater. Syst. Struct.* **14** 633–42

[45] Olsen Z J and Kim K J 2018 A reduced dimensional mapping approach for modeling IPMCs with computational efficiency and rapid design development applications *Smart Mater. Struct.* **27** 125012

[46] Cha Y, Aureli M and Porfiri M 2012 A physics-based model of the electrical impedance of ionic polymer metal composites *J. Appl. Phys.* **111** 124901

[47] Wallmersperger T, Kröplin B and Gülch R W 2004 Coupled chemo-electro-mechanical formulation for ionic polymer gels—-numerical and experimental investigations *Mech. Mater.* **36** 411–20

[48] Pugal D, Kim K J and Aabloo A 2011 An explicit physics-based model of ionic polymer-metal composite actuators *J. Appl. Phys.* **110** 084904

[49] Rossi M and Wallmersperger T 2018 Thermodynamically consistent three-dimensional electrochemical model for polymeric membranes *Electrochim. Acta* **283** 1323–38

[50] Nardinocchi P, Rossi M, Wallmersperger T and Ramirez Velazco J A 2018 Thermodynamically consistent electro-chemo-mechanical model for polymer membranes *Electroact. Polym. Actuators Devices XX* (*March*) p 18

[51] Wallmersperger T, Horstmann A, Kroplin B and Leo D J 2009 Thermodynamical modeling of the electromechanical behavior of ionic polymer metal composites *J. Intell. Mater. Syst. Struct.* **20** 741–50

[52] Nardinocchi P, Pezzulla M and Placidi L 2011 Thermodynamically based multiphysic modeling of ionic polymer metal composites *J. Intell. Mater. Syst. Struct.* **22** 1887–97

[53] Galante S, Lucantonio A and Nardinocchi P 2013 The multiplicative decomposition of the deformation gradient in the multiphysics modeling of ionic polymers *Int. J. Non-Linear Mech.* **51** 112–20

[54] Leichsenring P, Serdas S, Wallmersperger T, Bluhm J and Schröder J 2017 Electro-chemical aspects of IPMCs within the framework of the theory of porous media *Smart Mater. Struct.* **26** 045004

[55] Bufalo G D, Placidi L and Porfiri M 2008 A mixture theory framework for modeling the mechanical actuation of ionic polymer metal composites *Smart Mater. Struct.* **17** 045010

[56] Leronni A and Bardella L 2021 Modeling actuation and sensing in ionic polymer metal composites by electrochemo-poromechanics *J. Mech. Phys. Solids* **148** 104292

[57] Acartürk A Y 2009 *Simulation of Charged Hydrated Porous Materials* (Stuttgart: University of Stuttgart)

[58] Coussy O 2004 *Poromechanics* (New York: Wiley)

[59] Chapelle D and Moireau P 2014 General coupling of porous flows and hyperelastic formulations—from thermodynamics principles to energy balance and compatible time schemes *Eur. J. Mech.* B **46** 82–96

[60] Gurtin M E, Fried E and Anand L 2010 *The Mechanics and Thermodynamics of Continua* (Cambridge: Cambridge University Press)

[61] McMeeking R M and Landis C M 2005 Electrostatic forces and stored energy for deformable dielectric materials *J. Appl. Mech.* **72** 581–90

[62] Zhao X and Suo Z 2008 Electrostriction in elastic dielectrics undergoing large deformation *J. Appl. Phys.* **104** 123530

[63] Noll W, Coleman B D and Noll W 1974 The thermodynamics of elastic materials with heat conduction and viscosity *The Foundations of Mechanics and Thermodynamics* (Berlin: Springer) pp 145–56

[64] Coleman B D and Gurtin M E 1967 Thermodynamics with internal state variables *J. Chem. Phys.* **47** 597–613

[65] Liu I-S 2014 A solid–fluid mixture theory of porous media *Int. J. Eng. Sci.* **84** 133–46

[66] Liu I-S 1972 Method of lagrange multipliers for exploitation of the entropy principle *Arch. Ration. Mech. Anal.* **46** 131–48

[67] Liu I-S 1996 On entropy flux-heat flux relation in thermodynamics with lagrange multipliers *Contin. Mech. Thermodyn.* **8** 247–56

[68] Hauser R A and Kirchner N P 2002 A historical note on the entropy principle of Müller and Liu *Contin. Mech. Thermodyn.* **14** 223–6

[69] Truesdell C and Noll W 2004 *The Non-Linear Field Theories of Mechanics* (Berlin: Springer)

[70] Gajo A 2010 A general approach to isothermal hyperelastic modelling of saturated porous media at finite strains with compressible solid constituents *Proc. R. Soc.* A **466** 3061–87

[71] Karl T 1943 *Theoretical Soil Mechanics* (New York: Wiley)

[72] Onsager L 1931 Reciprocal relations in irreversible processes. I. *Phys. Rev.* **37** 405–26

[73] Onsager L 1931 Reciprocal relations in irreversible processes. II. *Phys. Rev.* **38** 2265–79

[74] Volpini V, Bardella L, Rodella A, Cha Y and Porfiri M 2017 Modelling compression sensing in ionic polymer metal composites *Smart Mater. Struct.* **26** 035030

[75] Pugal D 2012 *Physics Based Model of Ionic Polymer-Metal Composite Electromechanical and Mechanoelectrical Transduction* (Reno: University of Nevada)

[76] Nonner W, Peyser A, Gillespie D and Eisenberg B 2004 Relating microscopic charge movement to macroscopic currents: the Ramo-Shockley theorem applied to ion channels *Biophys. J.* **87** 3716–22

[77] Weber A Z and Newman J 2004 *Modeling Transport in Polymer-Electrolyte Fuel Cells* **104** 4679–726

[78] Ferguson T R and Bazant M Z 2012 Nonequilibrium thermodynamics of porous electrodes pp A1967–A1985

[79] Cha Y, Cellini F and Porfiri M 2013 Electrical impedance controls mechanical sensing in ionic polymer metal composites *Phys. Rev.* E **88** 062603

[80] Chen Z, Tan X, Will A and Ziel C 2007 A dynamic model for ionic polymer-metal composite sensors *Smart Mater. Struct.* **16** 1477–88

[81] Pugal D, Stalbaum T, Palmre V and Kim K J 2016 Chapter 5. Modeling ionic polymer metal composites with COMSOL: step-by-step guide *RSC Smart Materials* (Cambridge: Royal Society of Chemistry) pp 185–214

[82] Shen Q, Kim K J and Wang T 2014 Electrode of ionic polymer-metal composite sensors: modeling and experimental investigation *J. Appl. Phys.* **115** 194902

[83] Shen Q, Palmre V, Stalbaum T and Kim K J 2015 A comprehensive physics-based model encompassing variable surface resistance and underlying physics of ionic polymer-metal composite actuators *J. Appl. Phys.* **118** 124904

[84] Liu Y, Chang L, Hu Y, Niu Q, Yu L, Wang Y, Lu P and Wu Y 2018 Rough interface in IPMC: modeling and its influence analysis *Smart Mater. Struct.* **27** 075055

[85] Palmre V, Pugal D, Kim K J, Leang K K, Asaka K and Aabloo A 2014 Nanothorn electrodes for ionic polymer-metal composite artificial muscles *Sci. Rep.* **4** 6176

[86] Shahinpoor M and Kim K J 2000 The effect of surface-electrode resistance on the performance of ionic polymer-metal composite (IPMC) artificial muscles *Smart Mater. Struct.* **9** 543–51

[87] Arnoldus H F 2006 Conservation of charge at an interface *Opt. Commun.* **265** 52–9

[88] Gupta A and Steigmann D J 2009 Balance laws *Continuum Mechanics* ed J Merodio and G Saccomandi (United Kingdom: UNESCO Eolss Publishers) pp 120–40

[89] Slattery J C, Sagis L and Oh E-S 2007 *Interfacial Transport Phenomena* (Boston, MA: Springer US)

[90] Aris R 1962 *Vectors, Tensors and the Basic Equations of Fluid Mechanics* (New York, NY: Dover Publications Inc)

[91] McConnell A J 1957 *Applications of Tensor Analysis* (New York: Dover Publications Inc)

[92] Fried E and Gurtin M E 2007 Thermomechanics of the Interface between a body and its environment *Contin. Mech. Thermodyn.* **19** 253–71

[93] Cermelli P, Fried E and Gurtin M E 2005 Transport relations for surface integrals arising in the formulation of balance laws for evolving fluid interfaces *J. Fluid Mech.* **544** 339–51

[94] Hong W, Zhao X and Suo Z 2010 Large deformation and electrochemistry of polyelectrolyte gels *J. Mech. Phys. Solids* **58** 558–77

[95] Nardinocchi P and Pezzulla M 2013 Curled actuated shapes of ionic polymer metal composites strips *J. Appl. Phys.* **113** 224906

[96] Porfiri M, Leronni A and Bardella L 2017 An alternative explanation of back-relaxation in ionic polymer metal composites *Extrem. Mech. Lett.* **13** 78–83

[97] Boldini A and Porfiri M 2020 Multiaxial deformations of ionic polymer metal composites *Int. J. Eng. Sci.* **149** 103227

[98] Gantmacher F R 1960 *The Theory of Matricies* (Chelsea, Vermont: Chelsea Publishing Co)

[99] Revil A 2017 Transport of water and ions in partially water-saturated porous media. Part 1. Constitutive equations *Adv. Water Resour.* **103** 119–38

[100] Nemat-Nasser S, Zamani S and Tor Y 2006 Effect of solvents on the chemical and physical properties of ionic polymer-metal composites *J. Appl. Phys.* **99** 104902

[101] Fleming M J, Kim K J and Leang K K 2012 Mitigating IPMC back relaxation through feedforward and feedback control of patterned electrodes *Smart Mater. Struct.* **21** 085002

[102] Kilic M S, Bazant M Z and Ajdari A 2007 Steric effects in the dynamics of electrolytes at large applied voltages. II. Modified Poisson-Nernst-Planck equations *Phys. Rev.* E **75** 021503

[103] Porfiri M 2008 Charge dynamics in ionic polymer metal composites *J. Appl. Phys.* **104** 104915

[104] Buckingham E 1914 On physically similar systems; illustrations of the use of dimensional equations *Phys. Rev.* **4** 345–76

[105] Brand L 1957 The Pi theorem of dimensional analysis *Arch. Ration. Mech. Anal.* **1** 35–45

[106] Curtis W D, Logan J D and Parker W A 1982 Dimensional analysis and the Pi theorem *Linear Algebra Appl.* **47** 117–26

[107] Sonin A A 2004 A generalization of the Π-theorem and dimensional analysis *Proc. Natl Acad. Sci. USA* **101** 8525–6

[108] Cha Y and Porfiri M 2013 Bias-dependent model of the electrical impedance of ionic polymer-metal composites *Phys. Rev.* E **87** 022403

[109] Aureli M, Prince C, Porfiri M and Peterson S D 2010 Energy harvesting from base excitation of ionic polymer metal composites in fluid environments *Smart Mater. Struct.* **19** 015003